TRACKING OF CORONARY ARTERIES IN ANGIOGRAM SEQUENCE BY STRUCTURAL MATCHING OF JUNCTIONS

WANG YUMEI

NATIONAL UNIVERSITY OF SINGAPORE

2011

TRACKING OF CORONARY ARTERIES IN ANGIOGRAM SEQUENCE BY STRUCTURAL MATCHING OF JUNCTIONS

WANG YUMEI (HT080162U)

(B.Sc., FUDAN UNIVERSITY, CHINA, 2008)

A THESIS SUBMITTED

FOR THE DEGREE OF MASTER OF SCIENCE

DEPARTMENT OF COMPUTER SCIENCE

SCHOOL OF COMPUTING

NATIONAL UNIVERSITY OF SINGAPORE

AUGUST 2011

Acknowledgement

Contents

Abstract

Coronary artery disease is the most common form of heart disease and is a leading cause of death worldwide. The standard diagnostic tool for coronary artery disease is x-ray angiography. Angiogram sequences are routinely captured for diagnosis and treatment of coronary artery diseases. As angiograms are 2D images, it is useful to reconstruct the 4D (3D-plus-time) structure of coronary arteries to better assist the cardiologist in diagnosis and treatment. To achieve this goal, it is necessary to track the coronary arteries in the angiogram sequences. However, it is a very difficult and challenging task because the arteries become visible and later invisible as contrast agent flows through them. Moreover, they change shape over time due to the motion of the heart and the chest.

To address these issues, this thesis proposes a novel method that automatically tracks major junctions of the blood vessels. It automatically extracts the blood vessel branches and junctions. A junction is characterized by a descriptor vector of the angles and widths of every branch of the junction. Junctions are tracked by matching their descriptors in successive angiogram frames. Also, an augmented graph is constructed to represent the connectivity patterns of the junctions in each frame. Then, the augmented graphs are used to disambiguate between possible candidate matches and estimate the locations of missing junctions.

The algorithm is applied to 6 angiogram sequences that are taken for one patient in different view points. Test results show that the algorithm can correctly track most of the junctions most of the time.

List of Tables

List of Figures

Chapter 1

Introduction

1.1 Motivation

Coronary artery disease is the most common form of heart disease and is a leading cause of death worldwide. It is one of the root causes of chest pain, heart failure and abnormal heart rate. As reported by National Center for Health Statistics, 25.4% of the total deaths in US is caused by coronary artery disease [44]. In coronary artery disease, a combination of fatty material, calcium, and scar tissue builds up in the arteries and causes the narrowing or blockage of the arteries. If this situation is not treated, it will lead to heart muscle damage or death in the long term.

The standard diagnostic tool for coronary artery disease is x-ray angiography. In x-ray angiography, a patient is placed on a bed between a C-arm device (Figure 1.1). The C-arm has an x-ray source and a fluorescent screen on its two ends. A catheter is inserted into the patient's artery and a radio-opaque contrast agent is injecting into the patient's blood. As the contrast agent flows through the arteries, the blood vessels can be visualized on the angiogram images generated by the C-arm.

Angiograms are 2D images. To better understand the 3D structure of coronary arteries, angiogram sequences are often taken at different view points by rotating the C-arm around the patient's chest (Figure 1.1). Two approaches have been investigated to reconstruct a 3D model of the coronary arteries: biplane angiography and rotational angiography. Biplane angiography uses a special equipment with two x-ray sources and two sensors to take the x-ray images at two different view points simultaneously [6, 11, 20, 36]. Then, the images at two

1

Figure 1.1: Angiography device: C-arm (Image from http://www.medical.siemens.com).

view points can be used to reconstruct 3D model of the coronary arteries. Rotational angiography takes the angiogram sequences by performing a continuous rotation of C-arm around the patient [3, 22, 40, 48]. As all view points are on the same plane, tomography technique can be applied to reconstruct the 3D model.

Biplane and rotational angiography have some shortcomings. Biplane angiography needs special equipment to capture two views of the coronary arteries at the same time. Rotational angiography exposes the patient to additional x-ray radiation. Both approaches are not routinely applied in clinical practice. It would be clinically more useful to reconstruct a 3D model of coronary arteries using multi-view angiograms that are routinely captured in clinical practice.

A 3D model is stationary and lacks dynamic information of coronary arteries. A 4D (3D plus time) model provides complete information about the coronary arteries. To obtain a 4D model, two important steps are needed: (1) track the coronary arteries within each angiogram sequence and (2) establish correspondence between coronary arteries in different views. This thesis focuses on the first step.

Four image frames from an angiogram sequence are shown in Figure 1.2. They show the different states of the coronary arteries when the contrast agent flows through them. From the images, we observe the following characteristics of the angiogram sequences:

(a)   (b)

(c)   (d)
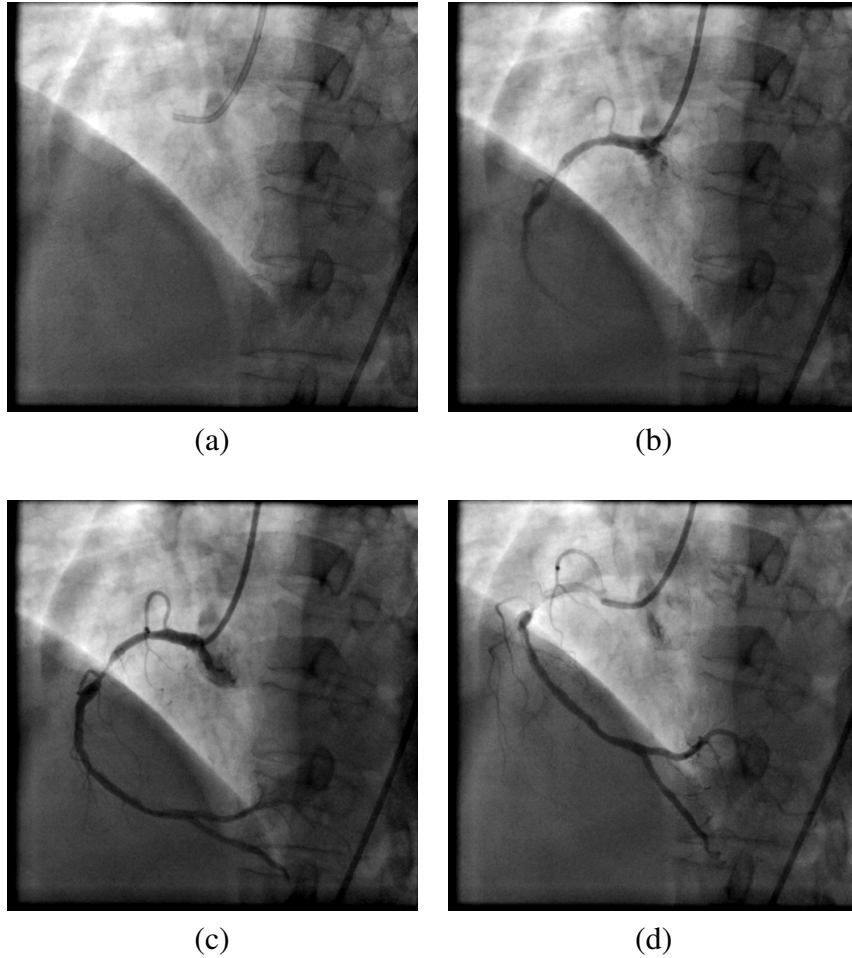
Figure 1.2: Frames from heart angiogram sequence.

- Blood vessels appear and disappear with contrast agent in the blood.
- Blood vessels' intensities and apparent widths change over time.
- Blood vessels' shapes change over time due to motion of heart and chest.

Therefore, tracking of blood vessels in angiogram sequences is a very difficult and challenging task.

A number of methods have been developed for blood vessel tracking. They can be categorized into two groups: elastic skeleton method [7, 28, 38, 39, 46, 47] and landmark tracking method [1]. Elastic skeleton method regards blood vessels as active curves and deform the curves in the current frame to match the curves in next frame. In general, active curves are sensitive to noise and changes of intensity and shape of the blood vessels. They require the user to initialize the active curves manually, and they typically track only one blood vessel branch at a time.

Landmark tracking method tracks distinct landmarks such as junctions of blood vessels instead of the whole blood vessels. To our best knowledge, there

is only one work that uses landmark tracking method [1]. It requires the user to indicate the location of a junction to be tracked. It characterizes a junction by its locations and angles between the branches, and tracks the junction by searching for a corresponding junction in the next frame with similar branch angles. Thus, it is less sensitive to intensity change. However, it is unable to identify the correct match when multiple junctions with similar branch angles are present in the next frame. Moreover, it can lose track when one or more branches of a junction disappear as the contrast agent exits the blood vessels.

To address these issues, this thesis proposes a novel method that automatically constructs and tracks the tree structure of junctions. It defines a more robust descriptor for tracking blood vessel junctions. In contrast to the existing junction tracking method, our method tracks the junctions without user inputs. Robust matching of shape descriptor is used, so it is less sensitive to intensity and shape change of junctions. Moreover, our method constructs an augmented graph that describes the connectivity pattern of the blood vessel branches in each frame. It uses the augmented graphs to disambiguate between possible candidate matches and estimate the possible locations of missing junctions. Compared with existing methods, our method is more practical, accurate and robust.

1.2   Thesis Objectives

The objective of this thesis is to develop an algorithm to track the blood vessels in the angiogram sequences. The algorithm requires the following properties:

- The algorithm should be effective and efficient.
- The algorithm should require none or fewer user inputs.

The most distinguishing parts of the coronary arteries are the junctions of the blood vessels. Furthermore, the structure of the entire coronary arteries is determined by the connection and position of the junctions. Therefore, this thesis focuses on tracking the junctions.

In this thesis, blood vessel extraction is based on the blood vessel enhancement method developed by Frangi et al. [10]. With the extracted blood vessels, a novel junction tracking method is developed based on the tree structure of junctions. The contributions of this thesis are as follows:

- Development of robust and accurate method for tracking junctions constrained by structural information of the blood vessels.
- Integrated the tracking method into a fully automatic blood vessel extraction and tracking algorithm.

1.3   Thesis Organization

Existing blood vessel extraction and tracking algorithms are reviewed in Chapter 2. The details of our method are discussed in Chapter 3. The method consists of three stages: multi-scaled image enhancement (Section 3.1), junction extraction (Section 3.2) and junction tracking (Section 3.3). The tracking method is applied to six angiogram sequences and results are shown and discussed in Chapter 4. Finally, conclusion is given in Chapter 5.

Chapter 2

Literature Review

Blood vessel tracking finds the corresponding points of the blood vessels in a temporal image sequence. A number of methods have been developed for finding corresponding points in blood vessel image registration [2,5,14,41,45]. However, blood vessel tracking is a different problem from registration. In registration, the input images are usually captured in different views. The difference between images is due to change of view points and can be large. For blood vessel tracking, the input images are adjacent frames in a temporal sequence. The difference between images is due to the motion of blood vessels and is usually small between consecutive images. However, there is a large number of frames in an image sequence, and the blood vessels may change intensity and shape as is the case for angiogram sequence. Therefore, only relevant methods for blood vessel tracking are discussed in this section.

Before blood vessels can be tracked, they must be extracted from the input image or image sequence. So, this chapter first presents a brief summary of existing blood vessel extraction algorithms (Section 2.1), followed by a more detailed review of existing blood vessel tracking algorithms (Section 2.2).

2.1 Blood Vessel Extraction Algorithms

Various techniques have been developed for blood vessel extraction. Existing techniques include snake, level set, tracking-based, artificial intelligence, and matched filtering. Kirbas and Quek published a detailed review and comparison of all these methods [16]. This section presents a brief summary of these methods.

In snake methods, the contours of blood vessels are modeled as active curves that deform under the influence of internal and external forces [17,21,33]. When these forces are balanced and the energy is minimized, the active curves should approach the contours of the blood vessels. These methods have some intrinsic shortcomings. For example, they are very sensitive to initialization and noise.

Level set methods represent the contours of blood vessels in 3D by a level set function [25, 31, 35]. This function is the signed distance function to the contours and it keeps all possible states of the blood vessels' contours. Hence, the propagating velocity of the contours is captured implicitly in the level set function. In the level set method, starting from a small circle within the vessel, it propagates to fit the boundaries of the blood vessels. It is useful for extracting blood vessels with complex topology. However, it is prone to leaking into undesired regions.

Tracking-based methods start from a set of seed points in the central axis of the blood vessels and trace the corresponding branches of the blood vessels iteratively [12, 24, 42]. For each seed point, the vessel width and direction are initialized either manually or automatically. Starting from the seed point, the method iteratively traces the next point in the central axis based on the direction of the current point. The new vessel width and direction of the new point is then computed from the local area of the image. This process is applied iteratively to trace the blood vessels. Tracking-based methods are intuitive and can extract the blood vessels efficiently. However, the disadvantage of tracing-based methods is that they requires user intervention to select the seed points.

Artificial intelligence methods utilize knowledge-based system to guide the blood vessel extraction [32, 37]. The knowledge of blood vessels is learned from the angiographic images and encoded in the form of a set of rules. For example, rules such as vessels have high intensity centerlines, comprise high intensity regions bordered by parallel edges, etc., are defined in the knowledge-based system of Smets et al. [37]. Based on these rules, the blood vessels are extracted accordingly. AI methods perform well in terms of accuracy, but they have high computational complexity compared with other methods.

Matched filtering methods extract blood vessels by detecting tubular features corresponding to blood vessels. These methods convolve the image with multiple matched filters tuned to respond to tubular patterns [13, 15, 26, 30]. Since the blood vessels in an image differs in orientations and sizes, it is crucial to design filters that respond to vessels with different orientations and sizes. Early matched filtering methods use fixed-sized filters to detect blood vessels [4, 29].

For example, Orkisz et al. [29] uses a median filter with a fixed size to extract vessels in different orientations. These single-scaled filters detect blood vessels that match the filters' sizes, but they have problems extracting vessels that vary in size. Multi-scaled filters were introduced to address this problem [10, 19, 23, 34]. In the method of Lorenz et al. [23], blood vessels are extracted by a non-linear multi-scaled filter based on the first derivative of Gaussian along a proper orientation. Another example is the multi-scaled Gabor filters of Sang et al. [34]. Their multi-scaled filters extract blood vessels in different sizes accurately in poor contrast and noisy background. As the matched filters are oriented, these methods can also detect the orientations of the blood vessels. Therefore, with well designed filters, matched filtering methods are capable of extracting blood vessels of different sizes and orientations accurately and automatically.

Among the existing methods, matched filtering methods are the most robust methods. Compared with other methods, they can extract blood vessels accurately and automatically even in noisy background. One example of these methods is developed by Frangi et al. [10]. Their method computes the Hessian matrix of image by convolving the image with second derivatives of Gaussian kernels. Principal component analysis is applied to the Hessian matrix. The principle directions give the orientation of the blood vessels while the eigenvalues give the likelihood of the existence of true blood vessels. Finally, the filter responses of different scales are integrated to form the final filtering result. In this thesis, we use this method to extract the blood vessels. Details of Frangi's algorithm will be discussed in Chapter 3.

2.2   Blood Vessel Tracking Algorithms

Blood vessel tracking estimates the correspondence of blood vessels between adjacent frames. It can be used to obtain the dynamics of the coronary arteries. Existing methods for blood vessel tracking can be categorized into two groups:

- Elastic skeleton method
- Landmark tracking method

2.2.1 Elastic Skeleton Method

In elastic skeleton method, the center lines of blood vessels are regarded as active curves. The correspondence of blood vessels between successive image frames is estimated by deforming the curve in one frame to match that in the next frame. Curve deformation is regarded as an energy-minimization process, guided by external force and internal force. Elastic skeleton method can be divided into two groups: snake method and template string method.

Snake

In snake method, the center line of a blood vessel is a curve $\mathbf{s}$ represented by connected points $\mathbf{s}(i)$, $i \in [1, n]$ [7, 28, 38, 39]. The energy of the curve has two parts: the internal energy due to smoothness constraints and external energy due to image features:

$$E = E_{int} + E_{ext} \tag{2.1}$$

The internal energy is:

$$E_{int} = \sum_{i=2}^{n} (|D_i - D_{i-1}| + |k_1(i) - k_2(f(i))| + |f(i) - f(i-1)|) \tag{2.2}$$

where the first term $|D_i - D_{i-1}|$ is the motion smoothness constraint and D_i is the displacement of point $\mathbf{s}(i)$. The second term is the shape similarity constraint. It denotes the difference between the local curvatures at point $\mathbf{s}_1(i)$ and $\mathbf{s}_2(f(i))$, where $\mathbf{s}_2(f(i))$ is the correspondence of point $\mathbf{s}_1(i)$. The last term $|f(i) - f(i-1)|$ ensures the uniformity of matching, where $f(i)$ is the index of the point in $\mathbf{s}_2$ matched to $\mathbf{s}_1(i)$ (Figure 2.1). In traditional snake method, the external energy E_{ext} comes from the image intensity:

$$E_{ext} = \sum_{i=1}^{n} I(\mathbf{s}(i)) \tag{2.3}$$

where $I(\mathbf{s}(i))$ is the image intensities of the point $\mathbf{s}(i)$. This energy attracts the snake to low intensity regions that would be the center lines of blood vessels. When the energy E in Equation 2.1 is minimized, the snake is deformed to match the center line of the blood vessel.

With a good initialization and well defined energy function, the snake can deform well to fit the blood vessel. But it is sensitive to noise and large shape change of the blood vessel. To improve it, Fallavollita and Cheriet replace the
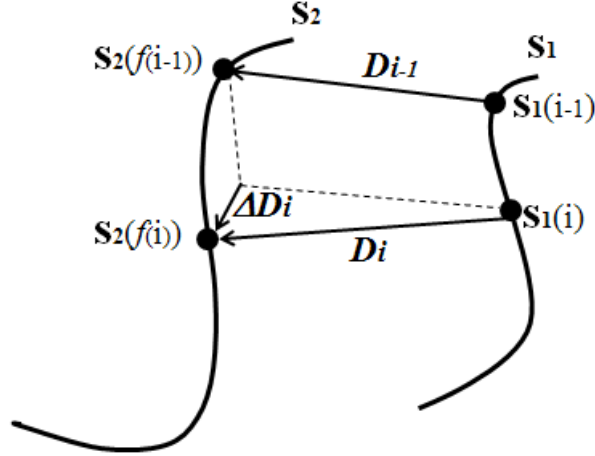
Figure 2.1: Internal energy of snake. Internal forces deform the center line of blood vessel in one frame to match that in next frame (Image from [38]).

usual external force by gradient vector flow field (GVF) [8]. GVF is a vector field derived from the diffusion of the gradient vectors of a gray-level or binary edge map derived from the image [43]. Although GVF is less sensitive to initialization than traditional snake, it still requires a good initialization and can also be distracted by noise.

Another problem of snake method is that the curve representing the blood vessel may shrink, grow or drift along the vessel from frame to frame. In these cases, snake method cannot guarantee correct tracking of the points in the blood vessel center line. Moreover, it can track only one blood vessel branch at a time.

Template String

To prevent shrinking, growing or drifting of the snake, template matching technique is included in the snake model to improve the external force [46, 47]. Template matching technique estimates the correspondence of interest points by applying a template of an interest point in current frame to match the interest point in the next frame. Generally, a template is represented by a window around the interest point in the image. In this way, the external energy term in 2.3 is replaced by:

$$E_{ext} = \sum_{i=1}^{n} (I_w(\mathbf{s}_t(i)) - I_w(\mathbf{s}_{t+1}(f(i))))$$ (2.4)

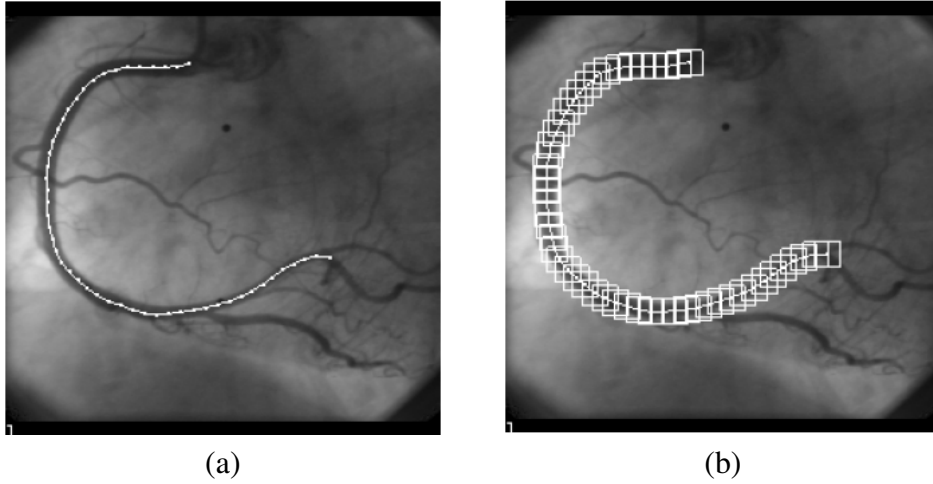<center>(a)   (b)</center>

Figure 2.2: Template string. (a) The snake of the blood vessel. (b) The template string of the blood vessel (Image from [47]).

where I_w is the template with width w around the point in the snake. $f(i)$ is the corresponding point of i. As shown in Figure 2.2, the blood vessel is no longer a snake curve, but a string of template windows. When minimizing the energy of this template string, the external force will pull that small window at each point to a best matching point in the next frame.

Template string method can solve the problem of shrinking, growing or drifting of the curve when tracking the blood vessel. However, it is sensitive to change in image intensity and large shape change of the blood vessel.

2.2.2   Landmark Tracking Method

Instead of tracking the whole blood vessel, an alternative is to track distinct landmarks of the blood vessels. For example, junctions of the blood vessels can be used as landmarks [1].

Bellemare et al. [1] represent the junction as a simple Y geometric structure (Figure 2.3). They manually select the junction and track it by looking for a similar Y shape in the next frame. The Y shape is geometrically defined by a descriptor of 5 parameters:

$$Y = (c_x, c_y, \theta_1, \theta_2, \theta_3) \tag{2.5}$$

The first two parameters are the coordinates of the junction's center point. The other three parameters are the three angles subtended by the branches of the

<center>11</center>
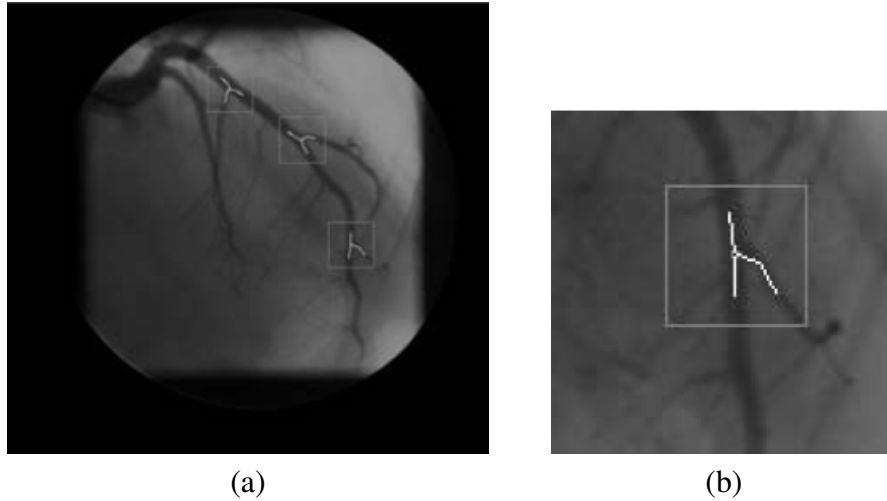
Figure 2.3: Junction Y shapes (Image from [1]).
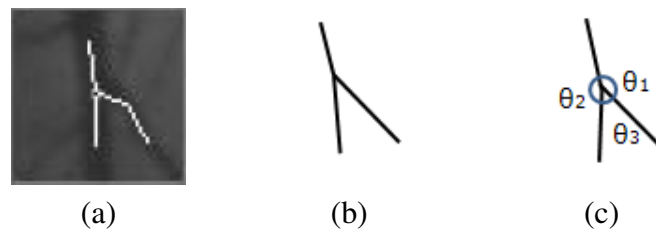
Figure 2.4: Junction descriptor. (a) The junction in the image. (b) The Y shape of the junction. (c) The descriptor of the junction.

Y shape (Figure 2.4). The correspondence of the junction is searched within a 50×50 pixels window centered at (c_x, c_y) in the next frame. The junction with the least sum of angle differences is selected:

$$min \sum_{i=1}^{3} |\theta_i(t) - \theta_i(t+1)| \tag{2.6}$$

Junction landmark tracking method is robust against intensity change and background noise. However, it is unable to identify the correct match when multiple junctions with similar branch angles are present in the next frame. Moreover, it can lose track when one or more branches of a junction disappear as the contrast agent exits the blood vessels.

Table 2.1: Comparison of blood vessel tracking methods.

Methods	Tolerance of intensity change	Tolerance of shape change	Tolerance of noise	Automatic
Elastic skeleton	N	N	N	N
Landmark tracking	Y	N	Y	N
Our method	Y	Y	Y	Y

2.2.3 Summary

In this section, existing blood vessel tracking methods are reviewed, which include elastic skeleton method and landmark tracking method.

Elastic skeleton methods regard blood vessels as active curves (i.e., snakes). They track the blood vessels by deforming and registering active curves to the centerlines of the blood vessels in each frame. In general, these methods are sensitive to noise and changes of intensity and shape of the blood vessels. They require the user to initialize the active curves manually, and they typically track only one blood vessel branch at a time.

Landmark tracking method uses junctions for tracking instead of the whole blood vessels. The existing method uses the junction center and branch angles as the descriptor of the junction. Thus, it is less sensitive to the image intensity change and noise. However, it is unable to identify the correct match when multiple junctions with similar branch angles are present in the next frame. Moreover, it can lose track when one or more branches of a junction disappear as the contrast agent exits the blood vessels.

The characteristics of existing blood vessel tracking methods are illustrated in Table 2.1. From the table, it is observed that a more robust method is needed to track the blood vessels automatically. The method should be invariant to the intensity change, noise and shape change of the blood vessel. Our proposed method satisfies all of these requirements.

Chapter 3

Proposed Tracking Algorithm

In contrast to existing methods, our method extracts the blood vessels and the junctions automatically. An image enhancement method is used to enhance the coronary arteries in the angiograms to facilitate the extraction of blood vessels and junctions. In addition, an augmented graph of the junctions is used to verify the matches and estimate unmatched junctions. Thus, our method is more robust than existing methods. The complete algorithm consists of three main stages:

- Multi-scaled image enhancement
- Landmark extraction and characterization
- Junction tracking

3.1 Multi-scaled Image Enhancement

In this stage, an angiogram image is enhanced using the method developed by Frangi et al. [10]. This method enhances tubular structures in different orientations and scales to facilitate the extraction of blood vessels and junctions in the next stage. It consists of three main steps:

- Image filtering by Gaussian derivatives
- Blood vessel enhancement in one scale
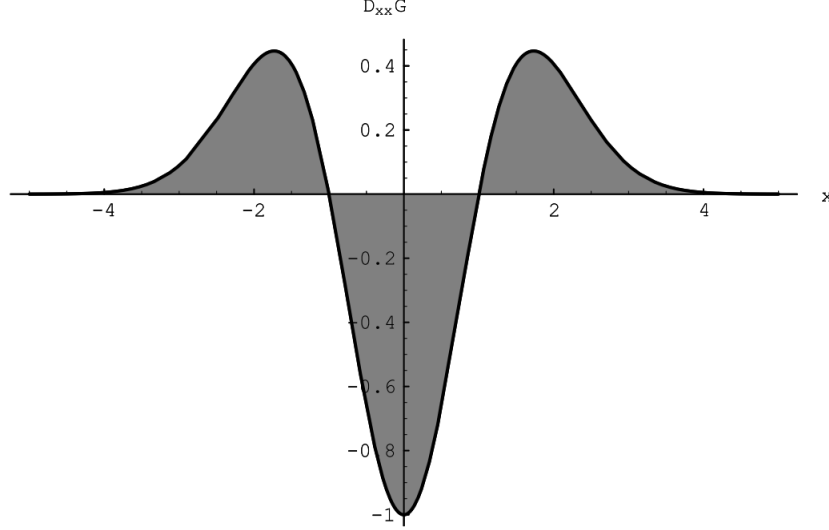- Integration of multi-scaled enhancements

Figure 3.1: The second-order derivative of a Gaussian kernel (Image from [10]).

3.1.1 Image Filtering by Gaussian Derivatives

To enhance the tubular structure in the image, the image is first filtered by the second derivatives of Gaussian to obtain the Hessian matrix of the image. The Hessian describes the intensity variation of the image:

$$\mathbf{H} = \begin{bmatrix} D_{xx} & D_{xy} \\ D_{xy} & D_{yy} \end{bmatrix} \tag{3.1}$$

$$D_{xx} = \frac{\partial^2 I}{\partial x^2}, \quad D_{xy} = \frac{\partial^2 I}{\partial x \partial y}, \quad D_{yy} = \frac{\partial^2 I}{\partial y^2}$$

where D_{xx}, D_{xy} and D_{yy} are the second-order partial derivatives of the image, respectively. In linear scale-space theory [9, 18], the derivative of image I at a point $\mathbf{p}$ is defined as a convolution with the derivatives of Gaussian $G(\mathbf{p}, s)$ at scale s:

$$\frac{\partial}{\partial \mathbf{p}} I(\mathbf{p}, s) = s^{\gamma} I(\mathbf{p}) \star \frac{\partial}{\partial \mathbf{p}} G(\mathbf{p}, s) \tag{3.2}$$

where the parameter γ defines a family of normalized derivatives.

As shown in Figure 3.1, the second-derivative of a Gaussian kernel at scale s gives a probe kernel that measures the intensity contrast in the direction of the derivative. This measure is small in the background where there is no tubular structure and lacks contrast. On the other hand, it has a large measure at a blood vessel of width $2s$. Therefore, the Hessian at scale s has a strong response for the blood vessels with scale s.

15

(a) Input

(b) D_{xx}
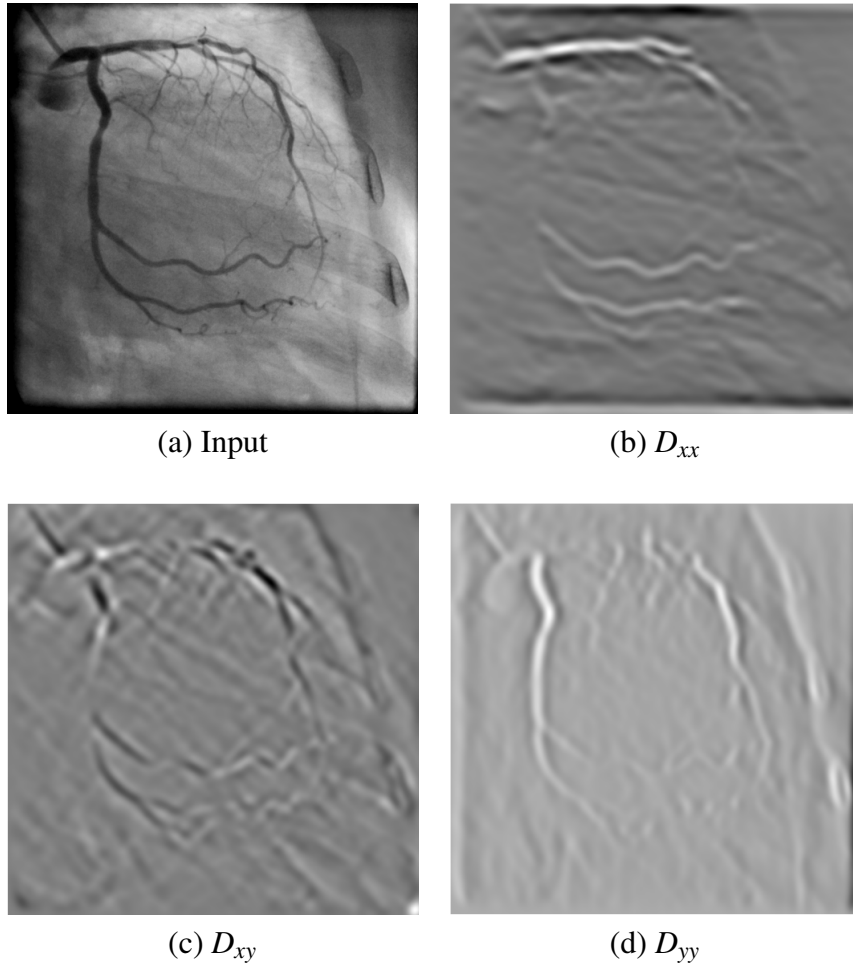
(c) D_{xy}

(d) D_{yy}

Figure 3.2: The second-order partial derivatives of the image.

3.1.2   Blood Vessel Enhancement in One Scale

The second-order partial derivatives of an image gives the intensity variation that implies the directions along tubular structures. Figure 3.2 gives the second-order partial derivatives, that is D_{xx}, D_{xy} and D_{yy} of an image at a certain scale. As shown in the figure, tubular structures in the directions of x-axis (horizontal), diagonal and y-axis (vertical) have a large response in the corresponding image. Therefore, it is intuitive to investigate the tubular structures in an image by analyzing its Hessian matrix.

The second-order structure of an image I in the neighbor $\delta\mathbf{p}$ of a point $\mathbf{p}$ is given in terms of its Hessian matrix:

$$\frac{\partial^2}{\partial(\delta\mathbf{p})^2}I(\mathbf{p}) = \delta\mathbf{p}^T\mathbf{H}\delta\mathbf{p} \tag{3.3}$$
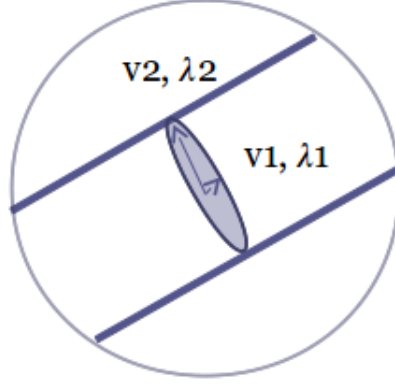
Figure 3.3: The eigenvectors of the Hessian locally. $\mathbf{v}_1$ and $\mathbf{v}_2$ indicate the directions along and perpendicular to a tubular structure. λ_1, λ_2 denote the corresponding eigenvalues, respectively.

Furthermore, from the definition of eigenvalues:

$$\mathbf{H}\mathbf{v}_k = \lambda_k \mathbf{v}_k \tag{3.4}$$

where λ_k denotes the corresponding eigenvalue of the k-th normalized eigenvector $\mathbf{v}_k$ of the Hessian $\mathbf{H}$. Multiplying Equation 3.4 with $\mathbf{v}_k^T$, we get:

$$\mathbf{v}_k^T \mathbf{H} \mathbf{v}_k = \lambda_k \tag{3.5}$$

The right side of Equation 3.3 is similar to the left side of Equation 3.5. The two equations imply that: $\mathbf{H}$ maps a spherical neighborhood centered at $\mathbf{p}$ onto an ellipse whose axes are along the direction of the eigenvectors of the Hessian and the axis's semi-length is the magnitude of the corresponding eigenvalues. This ellipse illustrates the local second-order structure of the image. As shown in Figure 3.3, $\mathbf{v}_1$ indicates the direction along a tubular structure with minimum intensity variation at scale s. λ_1, λ_2 denote the eigenvalues corresponding to the normalized eigenvectors $\mathbf{v}_1, \mathbf{v}_2$ of the Hessian.

The directions along and perpendicular to tubular structures can be determined from the local principal components of the Hessian. Particularly, a pixel belonging to blood vessels is signaled by λ_1 being small and λ_2 with a large magnitude. That is, the ideal tubular structure in the image should have

$$\begin{aligned} \lambda_1 &\approx 0, \\ \lambda_1 &\ll \lambda_2. \end{aligned} \tag{3.6}$$

Accordingly, a vessel pixel has a small ratio $R = \lambda_1/\lambda_2$ and the ratio R can be used to identify vessel pixels.

Blood vessel enhancement using only the ratio R is not sufficient. Background pixels may produce unpredictable enhancing response due to random noise fluctuations. The magnitudes of the derivatives (thus the eigenvalues) are small for background pixels. So, the measure

$$S = \sqrt{\lambda_1^2 + \lambda_2^2} \qquad (3.7)$$

can be used to distinguish noise from possible blood vessels. S is large for blood vessels and small for background pixels.

Combining the two components in Equation 3.6 and 3.7, blood vessel pixel **p** at a certain scale s is enhanced by the following vessel measure:

$$r(s) = \exp[-\frac{R}{2\alpha^2}][1 - \exp[-\frac{S^2}{2\beta^2}]] \qquad (3.8)$$

where α and β are thresholds controlling its sensitivity to the measures R and S. By using the product of the two measures, the response is maximal only if both of the two measures are satisfied, i.e., R is small and S is large.

3.1.3 Integration of Multi-scaled Enhancements

Blood vessels in an image have different scales. To have good enhancement results for all blood vessels, vessel measure in Equation 3.8 is applied at various scale to an image. The measure responses at different scales are integrated to obtain the enhanced result:

$$r = \max_{s_{min} \leq s \leq s_{max}} r(s) \qquad (3.9)$$

where s_{min} and s_{max} are the maximum and minimum scales of the blood vessels. They are chosen so as to cover the range of widths of blood vessels. The multi-scaled enhancement process is illustrated in Figure 3.4. The first four images show the vessel enhancement results obtained at increasing scales. The last image is the integrated result of the 4 enhancements using Equation 3.9.

Figure 3.5 shows a sample result of blood vessel enhancement. The left image is the input x-ray image. The right image shows the enhancement result. As shown in the figure, blood vessels at different scales are enhanced whereas
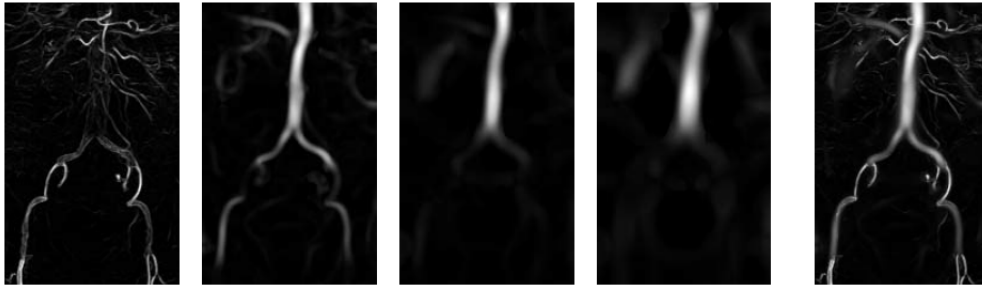
Figure 3.4: Multi-scaled enhancement illustration. The first 4 images show the vessel enhancement results obtained at increasing scales. The last one is the integrated result of the previous 4 enhancements (Image from [10]).

(a)   (b)
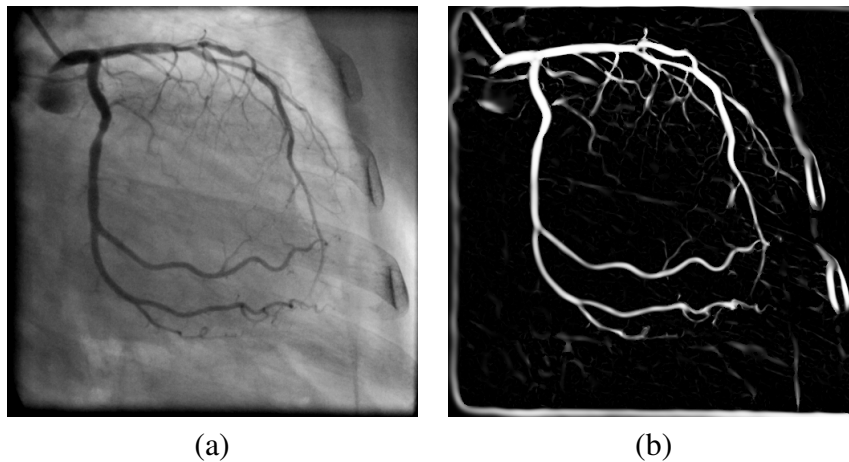
Figure 3.5: Multi-scaled filtering of blood vessel. (a) Input image. (b) Multi-scaled enhancement result.

the background is suppressed. However, some tubular backgrounds are also enhanced. For this step, the emphasis is to get as many blood vessels as possible. Noise will be filtered out in a later process.

3.2   Landmark Extraction and Characterization

This stage extracts the blood vessels and their junctions, and constructs the augmented graph. First, the enhanced image is turned into a binary image by thresholding. Next, the binary image is skeletonized and junctions and end points are extracted from the blood vessel skeleton and a junction graph is built
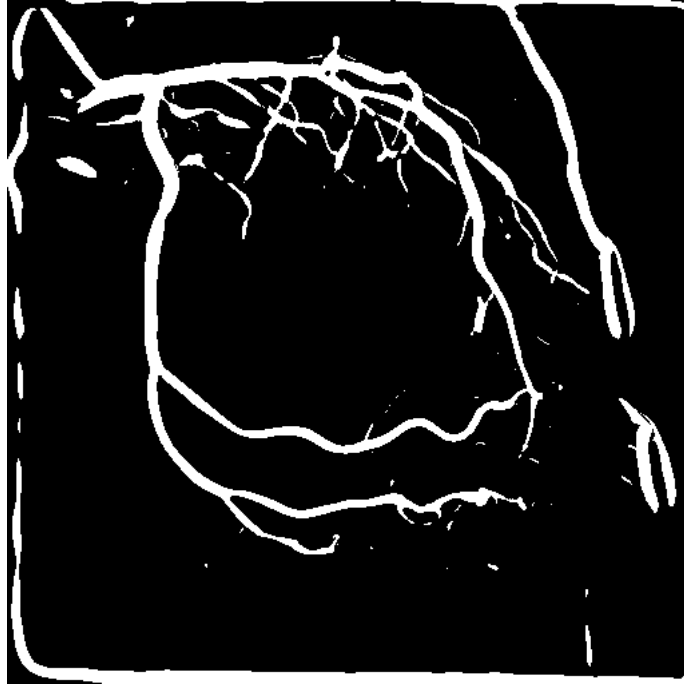
Figure 3.6: Binary image of blood vessel.

according to their connectivity in the blood vessels. Finally, the junctions are characterized by the branch angels and widths. There are four main steps in this stage:

- Image binarization
- Blood vessel skeletonization
- Landmark extraction
- Junction characterization

3.2.1 Image Binarization

After vessel enhancement, the processed image is still in gray scale and needs to be binarized before skeletonization. As the background has a lower intensity than the blood vessels, a small threshold is used to filter out the background. Most of the background regions can be filtered out using a threshold value of 0.2 for the intensity range of $[0, 1]$.

The binarization result is given in Figure 3.6. After thresholding, the resultant image is a binary image with white pixels for blood vessels and black pixels for background. Furthermore, the image boundaries are cropped to exclude noise since the blood vessels are all within the central area of the image.
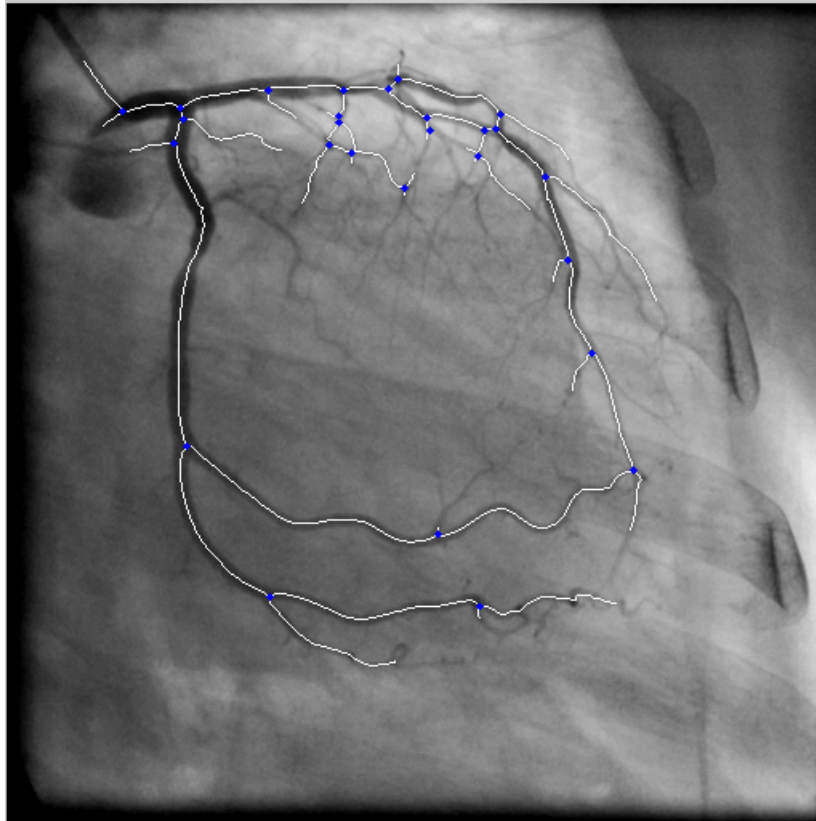
Figure 3.7: Blood vessel skeleton.

3.2.2   Blood Vessel Skeletonization

With the binary image, skeletonization is used to obtain the blood vessel
skeleton. The skeletonization technique used in this thesis is a morphological
operation. It is a useful tool in terms of extracting the geometrical structures
in a binary image. It analyzes the binary image by using a probe, a simple and
pre-defined shape, to detect components such as object boundaries or skeletons.

Skeletonization in morphology calculates the medial axis so that points on
this axis are at the same distance to its nearby borders. It is analogous to re-
moving pixels at the edges of an object simultaneously. The removal process
proceeds towards the center, without breaking the objects apart, until only sin-
gle pixel is left. The remaining pixels make up the object's skeleton.

In this thesis, we use the function *bwmorph* in Image Processing Toolbox of
MATLAB to do the skeletonization. After skeletonization, the blood vessels are
one pixel wide (Figure 3.7).

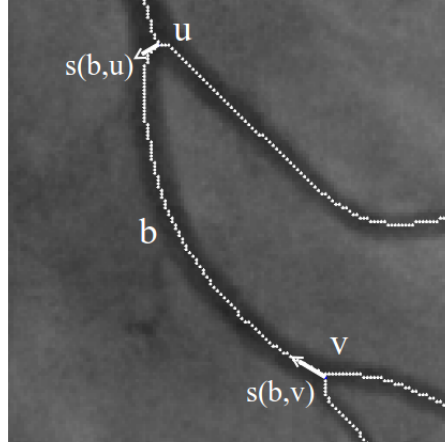Figure 3.8: Illustration of elements in the graph of junctions G. u and v are vertices. b is the branch that connects u and v. $s(b,u)$ and $s(b,v)$ are the branch segments of branch b at vertices u and v.

3.2.3   Landmark Extraction

In this step, junctions and end points are extracted and a graph of junctions is obtained by traversing the blood vessel skeleton. In the skeleton image, the skeleton point has value 1 while the background point has value 0. We define the connectivity of a skeleton point in terms of the number of skeleton points in its 8-neighborhood. That is, for a skeleton point with two neighboring skeleton points, it is a 2-connected point. In this context, there are three kinds of skeleton points in terms of their connectivity: (1) the end points of the skeleton are 1-connected, (2) the normal skeleton points are 2-connected, and (3) the junction points are k-connected where $k \geq 3$. For each junction point, we define this point together with its 8 neighbors as a junction block. In the case that several junction blocks overlap with each other, only the junction block with the most junction points is considered as a junction.

An augmented graph of junctions $G = (V, S, B)$ is obtained by traversing the blood vessel skeleton, where V is the set of vertices, S is the set of branch segments and B is the set of branches. A vertex $v \in V$ is either a junction or an end point. A branch segment $s \in S$ is a short segment attached to a vertex. It is characterized by its angle θ and width w. A branch $b \in B$ is a sequence of connected points between two vertices (Figure 3.8). Branch segments $s(b, u)$ and $s(b, v)$ are the short segments of branch b at vertices u and v. This graph records the connectivity information of junctions and end points. In addition, we define the path $P(u, v)$ as a connected sequence of branches from u to v, that
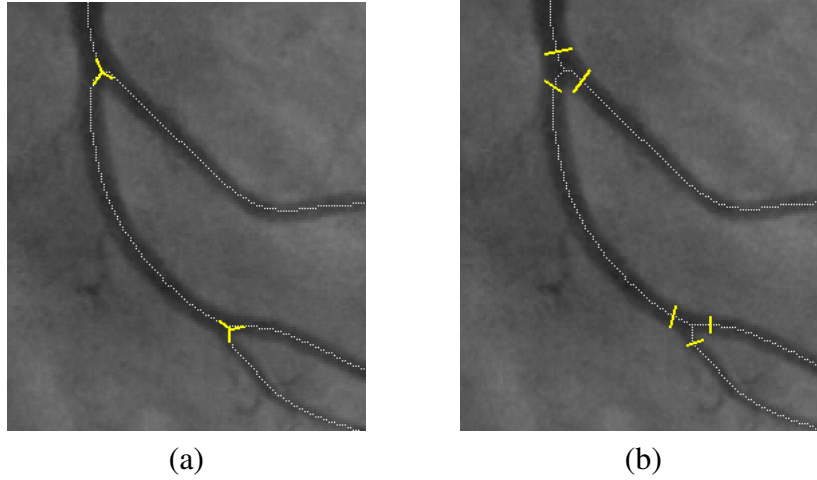
<div align="center">(a)   (b)</div>

Figure 3.9: Branch angles and widths of junctions. (a) The Y shapes give the angles of the junction. (b) The width of each branch is represented by the cross section.

is, $P(u, v) = \{b_1, ..., b_m\}$, $b_i \in B$, where b_1 is connected to u and b_m is connected to v.

3.2.4 Junction Characterization

A junction can be characterized by features such as its position, the intensity of its neighbors, its branch angles and branch widths. However, only the features that are invariant between adjacent frames are good for tracking. In this context, the position is not a good feature since it keeps changing throughout the sequence. The intensity of the block around a junction also changes because of movement of blood vessel and the flow of contrast agent. In contrast, the branch angles and widths change less significantly between two adjacent frames. Therefore, the branch angels and widths are then used to characterize the junction.

A junction v is characterized by the following feature descriptor D :

$$D(v) = (n, s_i, \overline{w}), i = 1, ..., n \tag{3.10}$$

where n is the number of branches, $s_i = (\theta_i, w_i)$ is the branch segment for the i-th branch, and $\overline{w}$ is the average branch width (Figure 3.9).

3.3　Junction Tracking

This section discusses the junction tracking algorithm. The junction is tracked by searching for a similar junction in the next frame. Similarity is measured by the difference of the two junctions' descriptors defined in Equation 3.10. In the following sections, an overview of our algorithm is first given, followed by details of each step.

3.3.1　Overview of Tracking Algorithm

For each frame i in the angiogram sequence, a graph of junctions G is obtained to characterize the blood vessels. Junction tracking aims at finding the correspondence between the junctions in the graphs G and G' of two consecutive frames.

In the angiogram sequence, the junctions appear and disappear when the contrast agent flows through the blood vessels. Therefore, we start the tracking from an intermediate frame that has the largest number of junctions in the sequence. Junctions are tracked frame by frame in forward and backward directions.

The overview of our tracking algorithm is given in Algorithm 3.1. There are three main stages in our tracking algorithm: matching, verification and estimation. In our algorithm, junctions in different statuses are defined as follows: matched junction is the junction having candidate correspondence, and confirmed junction is the junction whose correspondence has been confirmed by structural consistency.

Firstly, all the junctions are designated as unmatched junctions. In the matching step, candidate correspondences of junctions are first determined based on the difference $d(u, v)$ of the junction descriptors. Junctions with candidate correspondences are designated as matched junctions. After that, matched junctions are verified according to structural consistency of the junction graphs and designated as either confirmed or unmatched. Finally, the locations of unmatched junctions are estimated using structural information of the junction graphs.

24

Algorithm 3.1 Tracking junctions over frames.

---

1. Start with frame t that has the most junctions.

   All the junctions are designated as unmatched junctions.

2. Matching (Section 3.3.2):

   For each unmatched junction $u \in G$:
   - Find candidate correspondence $c(u) \in G'$. If $c(u)$ exist, u is called a unconfirmed (matched) junction.

3. Verification (Section 3.3.3):

   (a) Confirm the correspondence $c(u)$ of the junction u with the smallest match difference.

   (b) For each confirmed junction u:
   - Confirm the correspondence of its connected matched neighbors v based on structural consistency, if possible.
   - If confirmation is possible, designate v as confirmed. Otherwise, designate v as unmatched.

   (c) For each unconfirmed junction v:
   - Find a confirmed junction u along a connected path to confirm v's correspondence based on structural consistency, if possible.
   - If confirmation is possible, designate v as confirmed. Otherwise, designate v as unmatched.

   (d) Repeat at Step 3(b) until all unconfirmed junctions are designated as either confirmed or unmatched.

4. Estimation (Section 3.3.4):

   For each unmatched junction v:
   - Find confirmed junction u and the path P that connects u and v.
   - Mark corresponding position along corresponding path P' of P as $c(v)$.

5. Repeat for each frame in forward and backward direction.

3.3.2 Matching

This stage searches for the candidate correspondences of the junctions between two consecutive frames. The match difference between two junctions u and v with the same number n of branches is measured according to their descriptors:

$$d(u, v) = \alpha_1 \sum_{i=1}^{n} d(\theta_{u,i}, \theta_{v,i}) + \alpha_2 \sum_{i=1}^{n} |w_{u,i} - w_{v,i}| \qquad (3.11)$$

where α_1 and α_2 are the coefficients to balance the weights of the branch angle difference and the width difference. θ_i and w_i are the angle and width of the i-th branch segment s_i of junction u. Parameters α_1, α_2 are determined empirically and $\alpha_1 = 10$, $\alpha_2 = 2$ are used in this thesis. Branch angle difference between two angles θ_1 and θ_2 is computed as:

$$d(\theta_1, \theta_2) = \min(|\theta_1 - \theta_2|, 2\pi - |\theta_1 - \theta_2|) \tag{3.12}$$

For a junction u in G, the two most similar junctions in G' are detected within the search window 50×50 centered at the position of u in the next frame. Let v_1 and v_2 denote the two most similar junctions of u such that $d(u, v_1) < d(u, v_2)$. If $d(u, v_1) \leq \Gamma$ and there is $d(u, v_1) \ll d(u, v_2)$, then v_1 is a candidate corresponding junction of u, denoted as $c(u)$. u is called a matched junction. Otherwise, u has no candidate corresponding junction and it is called an unmatched junction. The threshold Γ is the nearest neighbor criterion. This criterion is applied to ensure that v is an unambiguous good match of u. In this thesis, threshold Γ is set as 0.8 empirically.

There are cases that more than one junction in G match the same junction in G'. In this case, we keep all the matches here and will determine the right correspondence in the verification step.

3.3.3 Verification

In the matching stage, candidate correspondences of the junctions in G have been determined. However, it is possible that two junctions having similar descriptors are actually not corresponding junctions (Figure 3.10). The tracking algorithm based on the junction descriptor alone will have problem in this case. To solve this problem, the method uses the structural consistency of the junction graph to verify the candidate correspondence of the junctions. This stage has four main steps and it is implemented with an ordered list R of confirmed junctions. R is initialized as an empty set.

Step (a) Since the junction u with smallest match difference is most likely to have correct match, its correspondence $c(u)$ is confirmed and u is added to R.
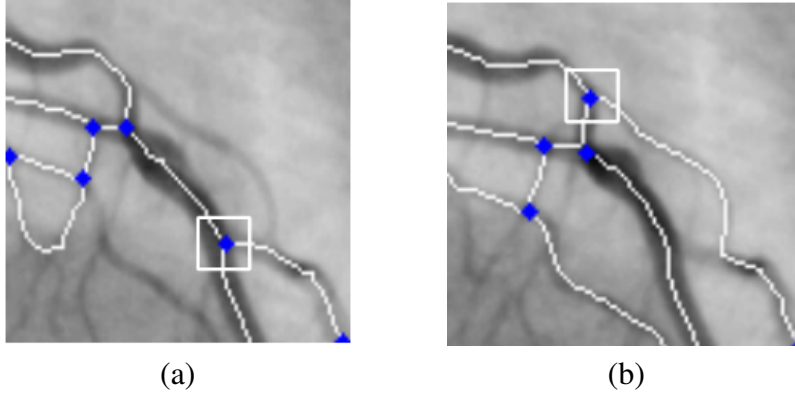
Figure 3.10: Different junctions with similar descriptors in adjacent frames. The two junctions marked by the white square in (a) and (b) have similar descriptors but not the same junction.

Step (b) The main idea is to propagate the confirmation of correspondence starting from confirmed junctions with small match differences, which are more likely to be correct matches. A junction in G' can only be the confirmed correspondence of a single junction in G. That is, good junctions and their immediate neighbors are given priority in confirming their matches. This method resolves the issue of multiple junctions in G matching the same junction in G'. This step is implemented using a first-in-first-out list R of confirmed junctions. A confirmed junction u is removed from R. Then, for each matched neighbor v of u, we first check if its correspondence $c(v)$ is occupied by any confirmed junction. If there is, $c(v)$ is discarded and v is designated as unmatched. Otherwise, we verify the correspondence of v by its confirmed neighbor u. The distance between junctions u and v connected by branch b is denoted as $d_b(u, v)$. It is defined as the length of branch b that connects them. We will confirm the correspondence of v and add it to R if:

$$d_b(u, v) \approx d_{c(b)}(c(u), c(v)) \tag{3.13}$$

where $c(u), c(v) \in G'$ are the correspondence of junctions $u, v \in G$, and $c(b) \in G'$ is the corresponding branch of branch $b \in G$ (Figure 3.11). If confirmation is possible, v is designated as confirmed. Otherwise, v is designated as unmatched. All junctions in R are processed until R is empty again.

Step (c) After Step (b), some unconfirmed junctions may remain unconfirmed because they are not reachable by a single branch. This step attempts to confirm these unconfirmed junctions by considering paths of more than one branch. It is
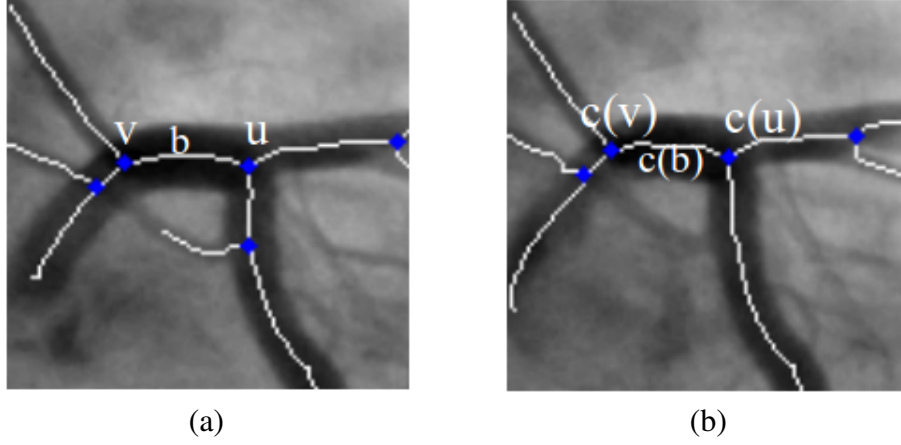
Figure 3.11: Verification of the correspondence of a junction. (a) Junctions in G. (b) Corresponding junctions in G'.

implemented using Breadth-First-Search (BFS). For each unconfirmed junction v in increasing match difference, we apply BFS to look for a confirmed junction u that is nearest to v in terms of the number of branches. Let $P(u, v) = \{b_1, ..., b_m\}$ denotes the shortest path from u to v where b_1 is connected to u and b_m is connected to v. and $P'(c(u), c(v)) = \{c(b_1),..., c(b_m)\}$ is the corresponding shortest path from $c(u)$ to $c(v)$. If the path difference $d(P, P')$ is small enough, then confirm the correspondence of u and add it to R. The difference between two paths is defined as:

$$d(P, P') = \alpha_1 |l(P) - l(P')| + \alpha_2 d(s(P), s(P')) \tag{3.14}$$

where α_1, α_2 are the coefficients to balance the weights of the length difference and the shape difference. The path length $l(P)$ is the sum of the lengths of branches in P. As the shape of the branches can change from one frame to the next, it is not necessary to compute detailed shape difference. Instead, the overall shape difference is measured in terms of the branch angles:

$$d(s(P), s(P')) = d(\theta(b_1), \theta(c(b_1))) + d(\theta(b_m), \theta(c(b_m))) \tag{3.15}$$

If confirmation is possible, v is designated as confirmed. Otherwise, v is designated as unmatched.

Step (d) After Step (c), additional matched junctions are confirmed. So, the algorithm repeats at Step (b) to propagate the confirmation of correspondence
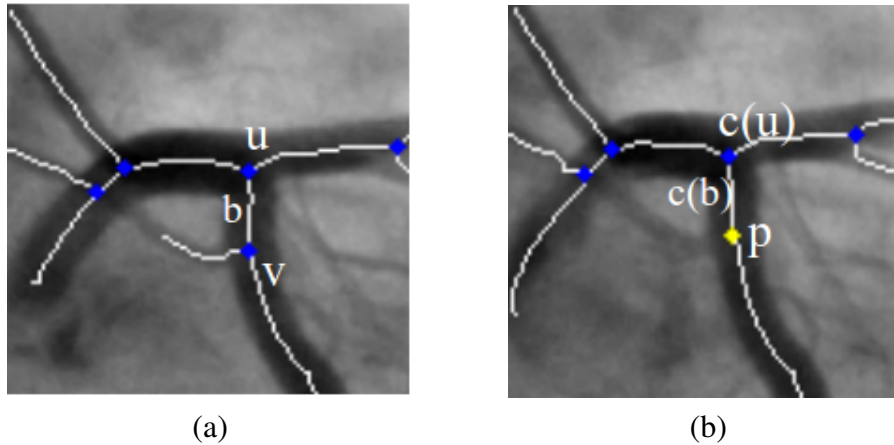
(a)   (b)

Figure 3.12: Junction estimation. (a) Junctions in G. (b) Corresponding junctions in G'.

from these confirmed junctions. This process iterates until all unconfirmed junctions are designated as either confirmed or unmatched.

After verification, mismatches with similar junction descriptors are discarded and all junctions are either confirmed junctions or unmatched junctions. The locations of unmatched junctions are estimated in the next stage.

3.3.4   Estimation

For the tracking of the junctions is performed in adjacent frames, if the tracking of a junction is lost (unmatched) in a frame, this junction will not be tracked in the remaining frames even it appears again. The lost of tracking happens due to the noise in angiogram images. If the tracking algorithm does not track the unmatched junctions, after some frames, only a small number of junctions are left for tracking. To address this problem, our algorithm estimates the locations of the unmatched junctions.

Similar to the verification stage, estimation of unmatched junctions makes use of the junction graph. For an unmatched junction v in G, we find a connected confirmed junction u with match $c(u)$ along path $P(u, v)$. To estimate the location $\mathbf{p}$ of junction v, we trace along the corresponding path $P'(c(u), \mathbf{p})$ in G' such that $d(P, P')$ is small enough. The path difference measure is the same as in Equation 3.14. If such a point $\mathbf{p}$ exists, a new junction is created and added to the junction graph G'. The descriptor of junction v is used as that of the new junction. Otherwise, the estimation fails and the algorithm will go on to next

estimation. An example of estimation is illustrated in Figure 3.12. In this case, the path P is a single branch b.

With the estimation, our algorithm is robust against the noise that causes missing junctions.

Chapter 4

Tests and Discussions

4.1   Input Data

In this thesis, the input data is 6 sequences of angiogram images of a patient captured in different time from different viewpoints. These images are from the National University Hospital (NUH) in Singapore. The coronary arteries in these six view points are shown in Figure 4.1. These are the standard view points used in clinic practice for diagnosing the coronary artery disease. There are around 50 frames for each sequence and each frame has a resolution of 512×512 pixels. All 6 sequences were sampled at 15 frames per second.

4.2   Experimental Results

The proposed junction tracking algorithm was tested on the 6 sequences of angiogram images. The results are shown in Table 4.1. The first row of the table gives the total number of junctions to be tracked in each sequence. The number of junctions detected in the 6 sequences ranges from 15 to 45. The second and third rows give the average and maximum duration (number of frames) in which the junctions appeared. The maximum duration ranges from 12 to 39, and the average duration ranges from 8.4 to 18.7. These results show that the angiogram sequences vary significantly.

In practice, a small amount of incorrect tracking can often be tolerated by using robust methods. So, tracking accuracy of a junction was measured in terms of the percentage of frames in which the junction was correctly tracked. The last

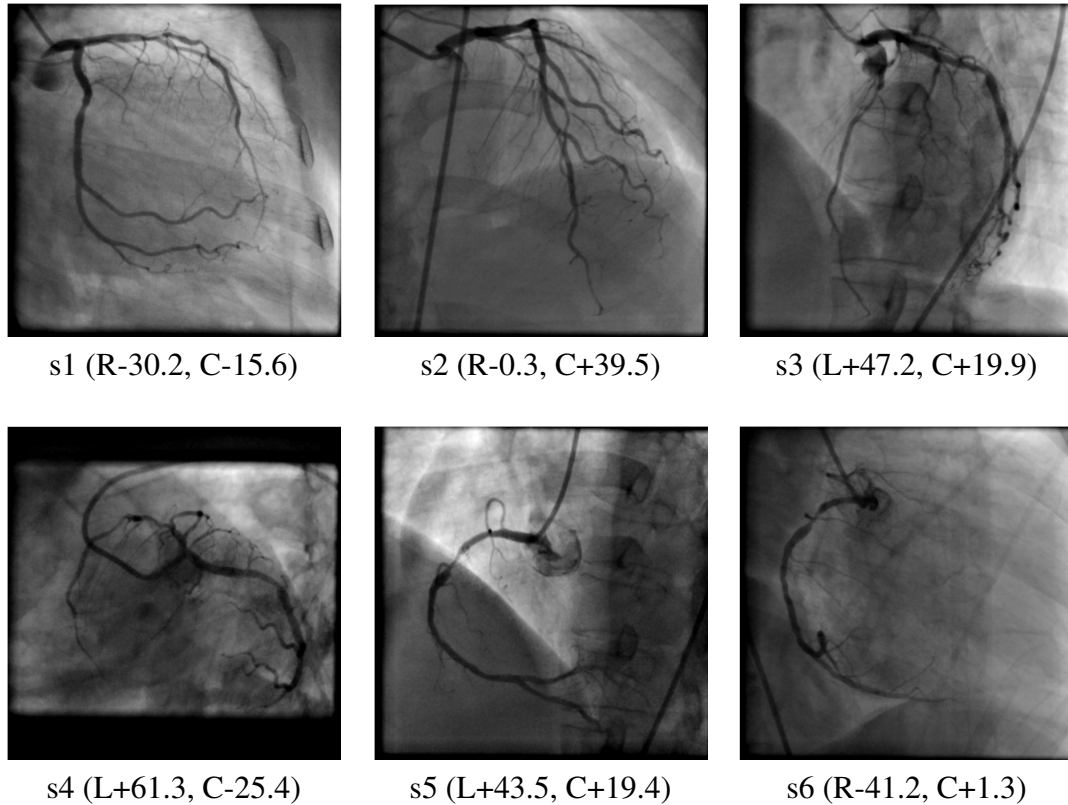|		
s1 (R-30.2, C-15.6)	s2 (R-0.3, C+39.5)	s3 (L+47.2, C+19.9)
s4 (L+61.3, C-25.4)	s5 (L+43.5, C+19.4)	s6 (R-41.2, C+1.3)

Figure 4.1: Coronary artery in 6 different view points, labeled from s1 to s6. The angles of the view points are given in the parentheses. L, R mean Left/Right Anterior Oblique angle respectively and C represents the Caudal angle.

three rows in Table 4.1 give the percentage of junctions that are tracked correctly in 100%, 90% and 80% of the frames in which they appeared respectively.

As shown in the table, for 4 of the 6 sequences, more than 86% of the junctions were correctly tracked in at least 80% of the frames. For the other 2 sequences, 67% and 76% of the junctions were correctly tracked in at least 80% of the frames. Overall, about 50% of the junctions were correctly tracked over 100% of the frames.

Two main factors contributed to the errors in junction tracking. The first factor is that the coronary arteries appear to overlap in 2D angiogram images, producing false junctions (Figure 4.2). As the heart beats, the arteries appear to move over each other. Consequently, the overlapping pattern changes, causing the sudden appearance and disappearance of false junctions. To resolve this problem, it is necessary to model the arteries as 3D structures whose 2D projections may overlap.

The second factor is due to the contrast agent. As the contrast agent enters two or more branches of the arteries, a junction appears. As it flows through

Table 4.1: Junction tracking results for 6 sequences.

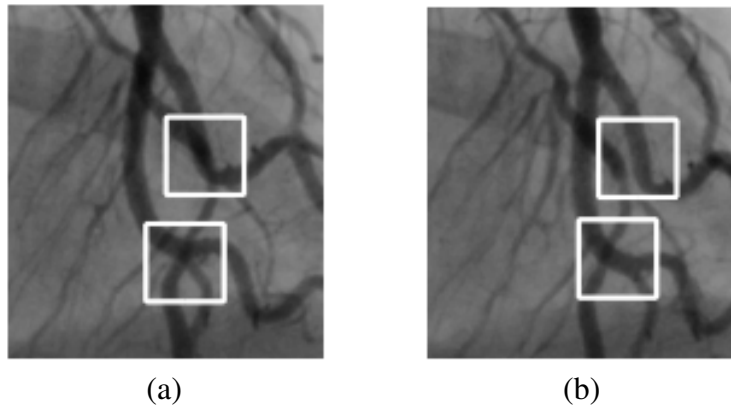|	s1	s2	s3	s4	s5	s6
# of junctions	45	34	27	15	16	15
mean duration	18.7	8.4	11.5	10.1	12.2	10.7
max duration	39	29	30	12	19	20
80%-correct	88.9	76.5	66.7	100.0	93.8	86.7
90%-correct	68.9	67.6	44.4	66.7	68.8	66.7
100%-correct	48.9	64.7	37.0	66.7	62.5	53.3

(a)   (b)

Figure 4.2: Overlap of blood vessels produces false junctions. Heart motion causes different parts of the blood vessels to overlap at different time, resulting in sudden change of the characteristics of false junctions (white boxes).

and exits the arteries, a junction may disappear in such a manner that causes the junction graph to break into two disconnected subgraphs (Figure 4.3 (a)), or a new branch may form at an existing junction (Figure 4.3 (b)), changing the characteristics of the junction. To handle this problem, it is necessary to perform error-tolerant subgraph matching [27] of the augmented graphs to account for the addition and deletion of branches and junctions. Error-tolerant subgraph matching is known to be computationally expensive.

This two factors both result in significant change of the structure of the junction graph. Experimental results show that 70% of the tracking errors is due to
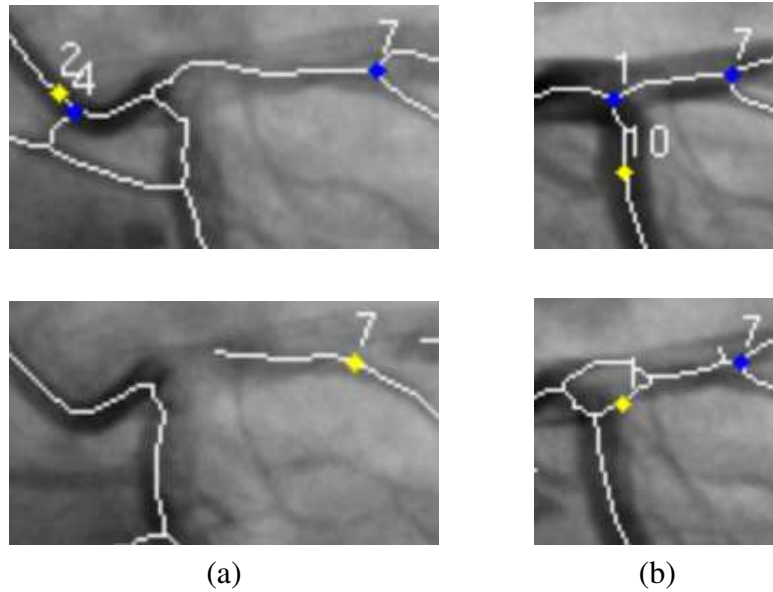
Figure 4.3: Flow of contrast agent causes apparent change of connectivity pattern. (a) Junction graph is broken into two unconnected subgraphs. (b) An additional branch is formed near junction 1.

overlapping of blood vessels and 30% is due to disappearance of contrast agent.

Our algorithm performs well when the structure of the blood vessels does not have significant change in adjacent frames.. Tracking results of four frames belonging to the same cardiac cycle in sequence 1 are shown in Figure 4.4 to Figure 4.7. The results show that our algorithm can track junctions correctly under significant change of image intensity and shape of the blood vessel.

The verification step in our algorithm assures the structural consistence of tracking result. To examine its effectiveness, the tracking result with and without the verification step is shown in Figure 4.8. As shown in the figure, without the verification step, the junction 30 is mismatched to a junction with similar branch angles and widths (Figure 4.8 (b)). With the verification, the mismatch is discarded and the junction 30 is estimated correctly (Figure 4.8 (c)).

Figure 4.9 shows the tracking results with estimating and without estimating the missing junctions. As can be seen in the figure, only a few number of junctions are left without estimating the missing junctions.

From the experiment results, it is concluded that our tracking algorithm can track the blood vessel correctly and automatically even with significant change of image intensity or shape of blood vessel. In addition, our algorithm is robust to deal with the missing junctions in certain frames. However, the change in
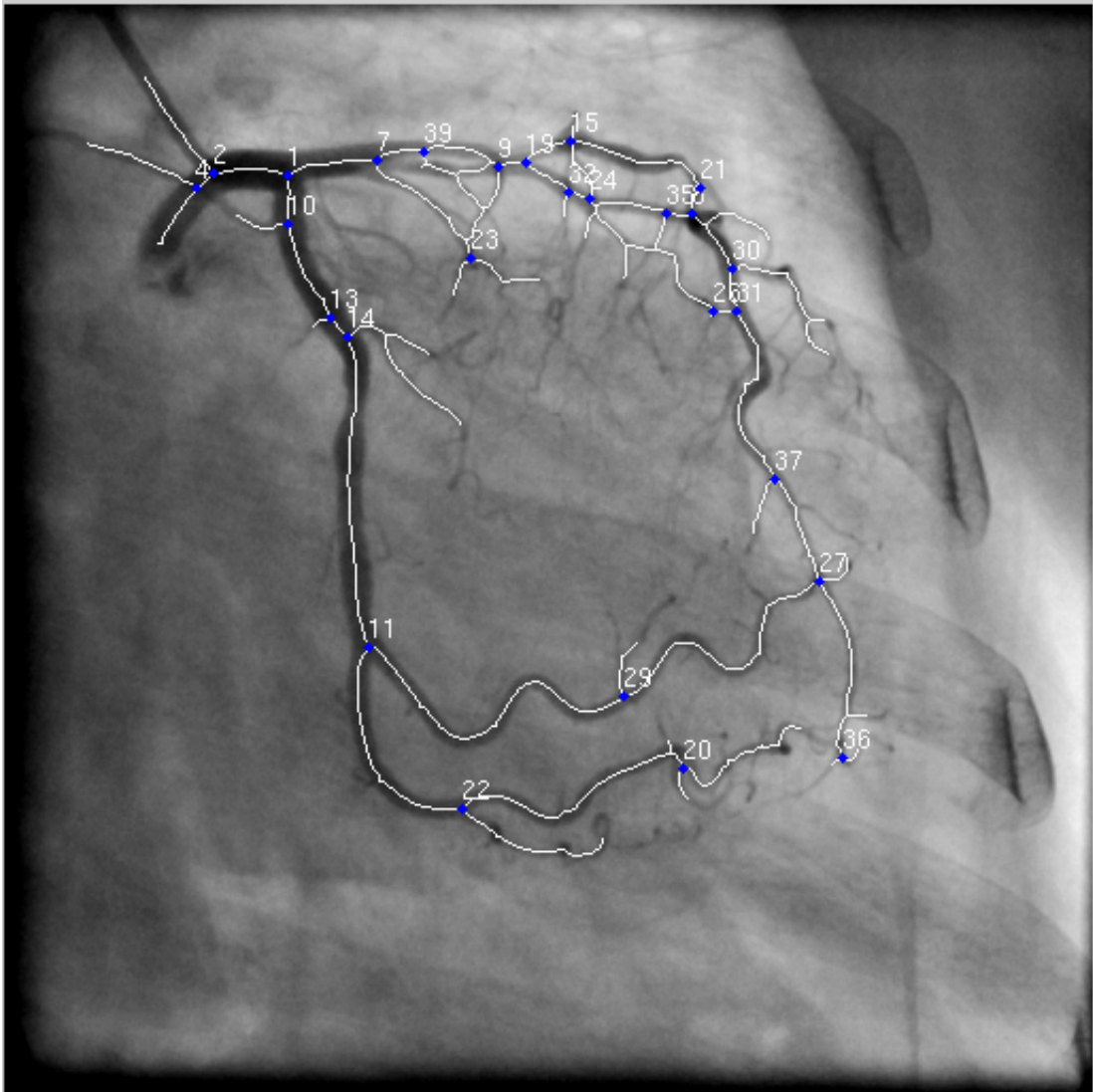
Figure 4.4: Start frame for tracking in sequence 1 (frame 30).

structure of blood vessels, that is, the junction graph, may interfere the performance of our algorithm.
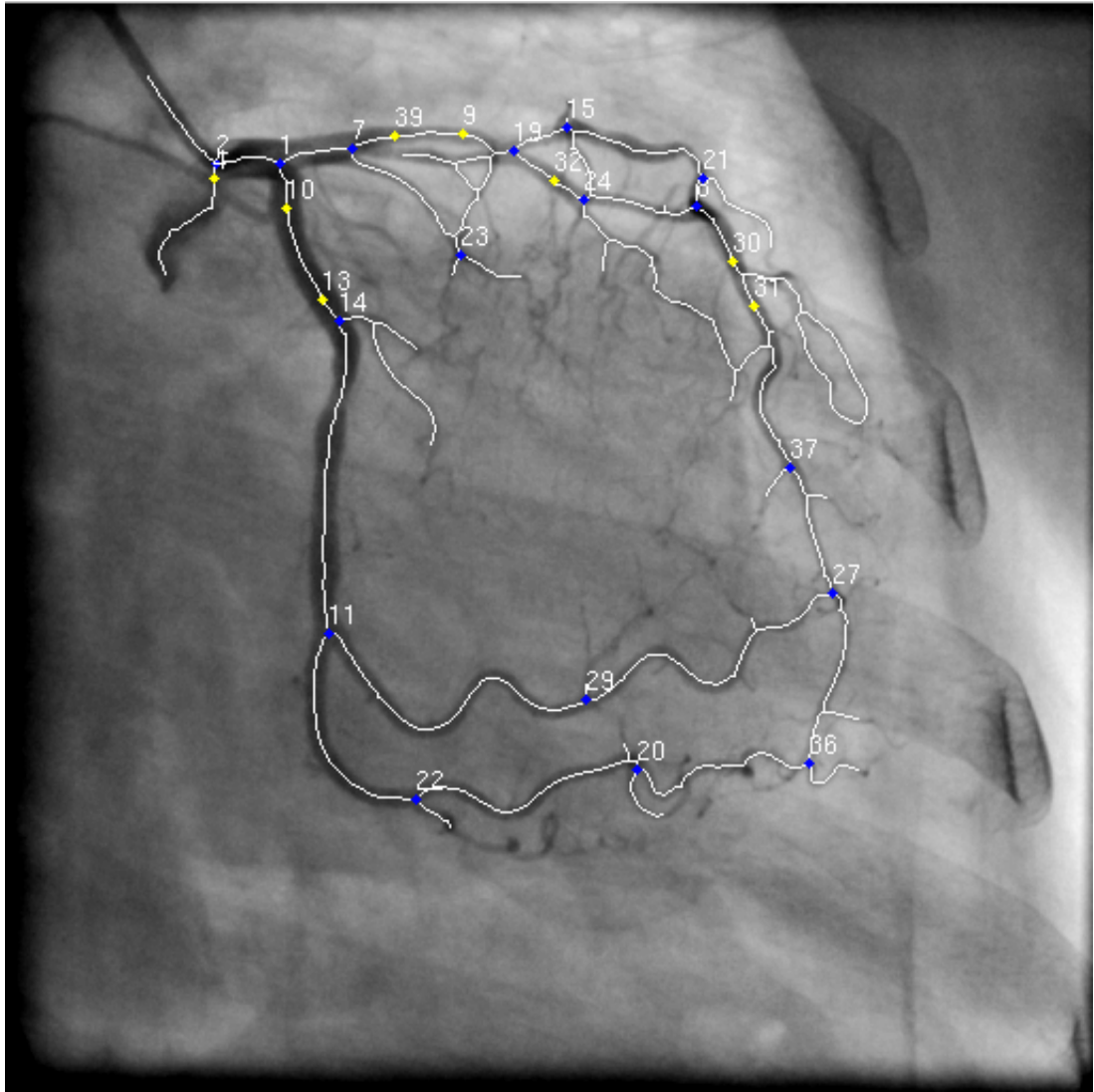
Figure 4.5: Tracking result in frame 32 in sequence 1.
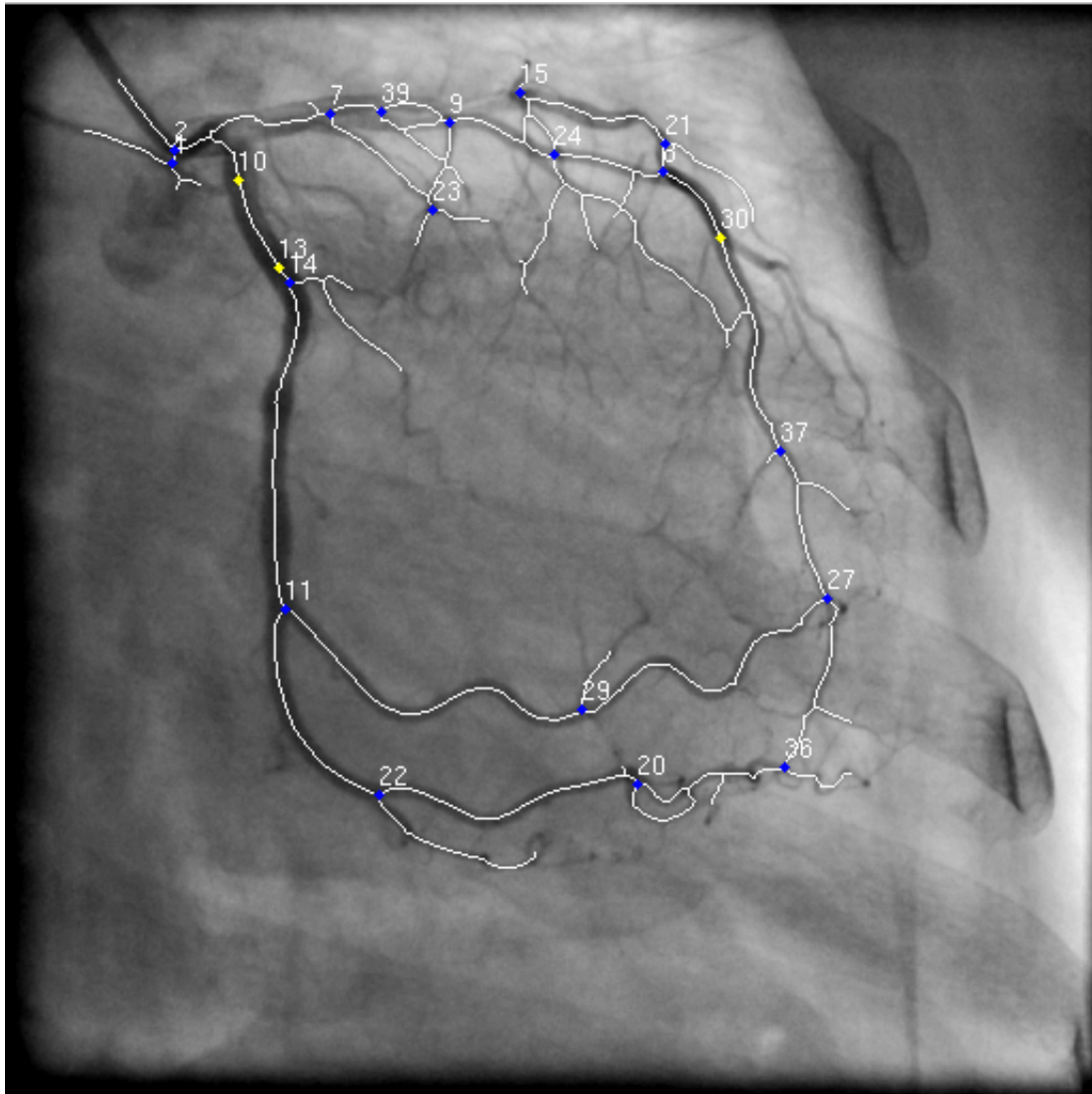
Figure 4.6: Tracking result in frame 34 in sequence 1.
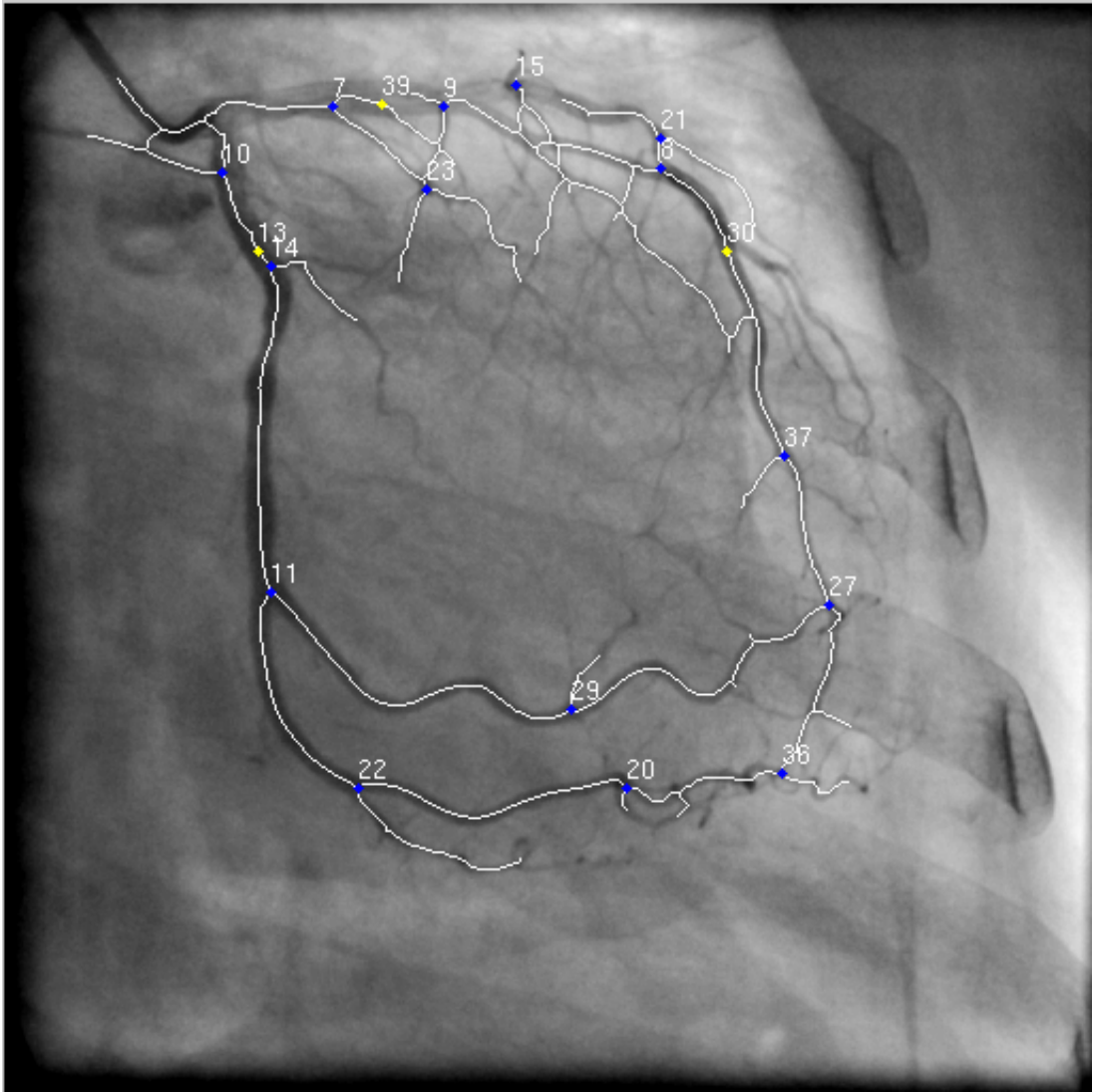
Figure 4.7: Tracking result in frame 36 in sequence 1.

(a)   (b)   (c)

Figure 4.8: Tracking results with and without verification. (a) The blood vessel in the input frame. (b) Without verification: the junction 30 is mismatch. (c) With verification: the mismatch is discarded and the junction 30 is estimated.

(a)

(b)

Figure 4.9: Tracking results with and without estimation after tracking for a few frames. (a) The tracking result without estimation. (b) The tracking result with estimation.

Chapter 5

Conclusion

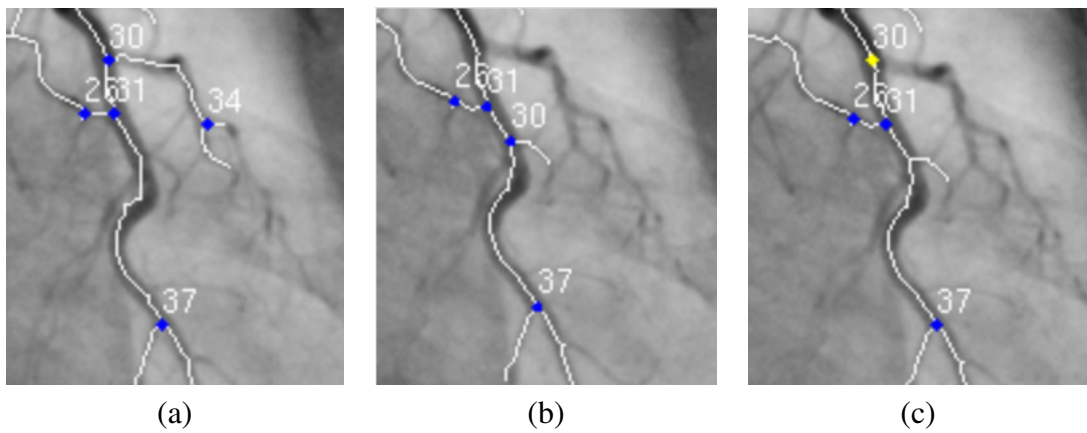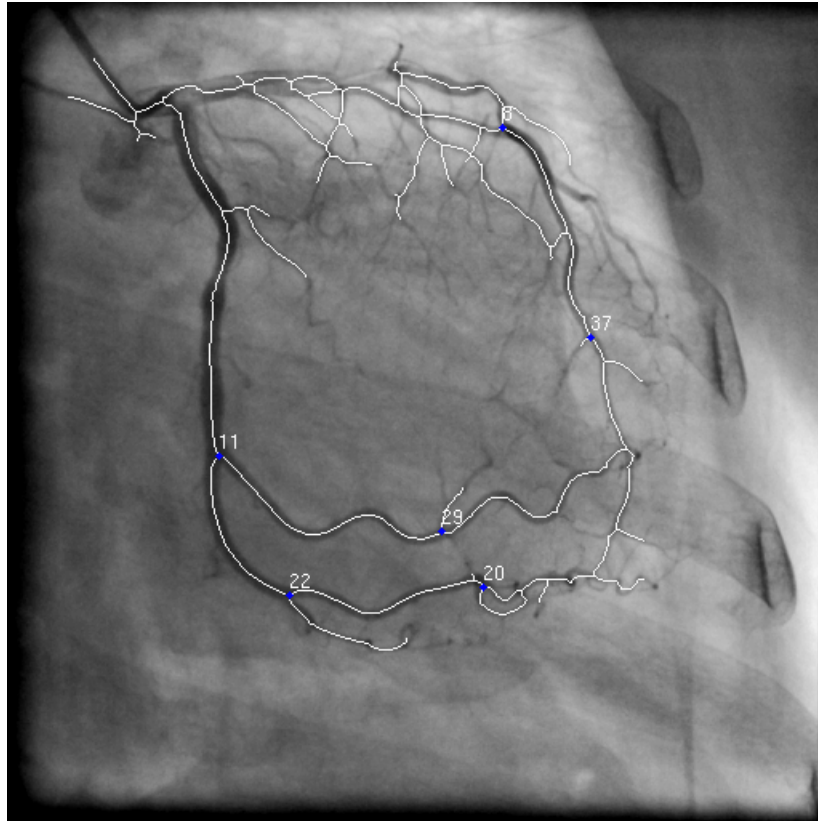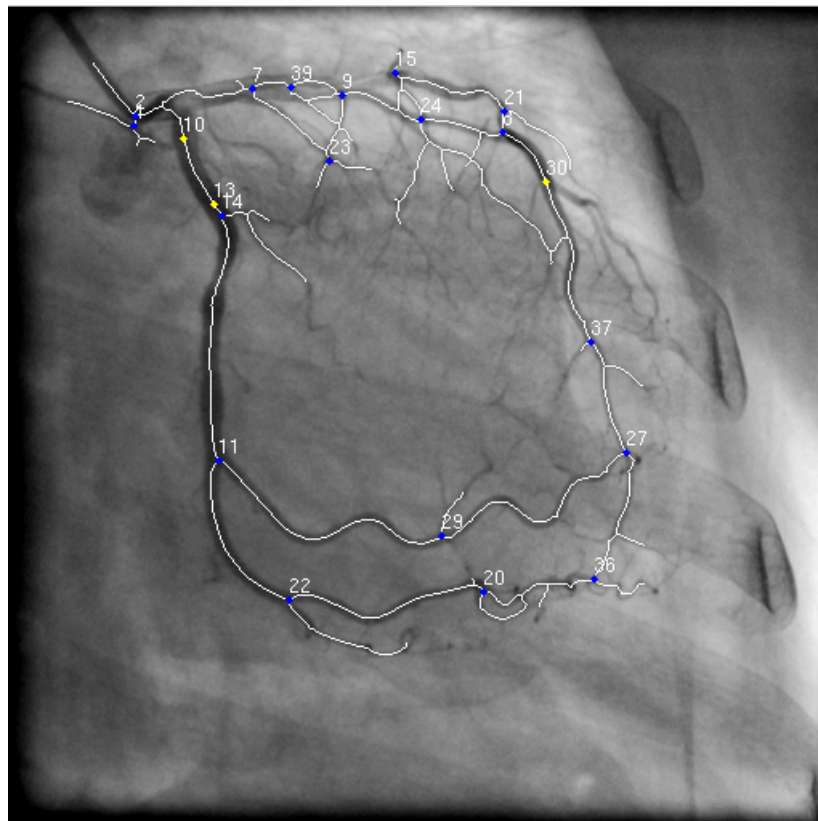Blood vessel tracking is an important step in 4D reconstruction of coronary arteries. Existing blood vessel tracking methods, such as elastic skeleton method and junction landmark method, can not handle the large shape change of the blood vessels and they all require user interaction in the tracking process.

This thesis presented an algorithm that automatically extracts coronary arteries in angiogram sequences and track the major junctions of the arteries within each sequence. Junction is distinguished feature for blood vessel tracking. In our algorithm, junctions are detected from the extracted blood vessel skeleton automatically. The branch angles and widths of the junction are used as its descriptor for junction tracking. An augmented graph is constructed to represent the connectivity patterns of the arteries in each frame. It is used to disambiguate between possible candidate matches, and to estimate the possible locations of missing junctions. Moreover, our algorithm estimates the location of missing junctions as a fallback on tracking failure.

Our algorithm tracks the junctions of blood vessels with a high accuracy. Compared with existing methods, it works well against significant change in the image intensity and the shape of blood vessels. In addition, it is more efficient since the tracking is only applied to the set of junctions rather than the blood vessels. Test results show that the algorithm can handle difficulties due to the flow of contrast agent in the arteries and motion of the heart. It can track most of the junctions correctly most of the time.

Bibliography

[1] C. Bellemare and J. Meunier. Structural method for tracking coronary arteries in coronary cineangiograms. In *Proc. of Canadian Conf. on Computer and Robot Vision*, pages 378–384, 2004.

[2] Y. Bentoutou, N. Taleb, M. Chikr El Mezouar, M. Taleb, and L. Jetto. An invariant approach for image registration in digital subtraction angiography. *Int. Journal of Pattern Recognition*, 35(12):2853–2865, 2002.

[3] C. Blondel, G. Malandain, R. Vaillant, and N. Ayache. Reconstruction of coronary arteries from a single rotational x-ray projection sequence. *IEEE Trans. on Medical Imaging*, 25(5):653–663, 2006.

[4] H. Chen and J. Hale. An algorithm for MR angiography image enhancement. In *Proc. of Int. Society for Magnetic Resonance in Medicine*, volume 33, pages 534–540, 1995.

[5] J. Chen, J. Tian, N. Lee, J. Zheng, R. T. Smith, and A. F. Laine. A partial intensity invariant feature descriptor for multimodal retinal image registration. *IEEE Trans. on Bio-Medical Engr.*, 57(7):1707–1718, 2010.

[6] S. J. Chen and J. D. Carroll. 3-D reconstruction of coronary arterial tree to optimize angiographic visualization. *IEEE Trans. on Medical Imaging*, 19(4):318–336, 2000.

[7] M. P. Dubuisson-Jolly, C. C. Liang, and A. Gupta. Optimal polyline tracking for artery motion compensation in coronary angiography. In *Proc. of Int. Conf. on Computer Vision*, pages 414–419, 1998.

[8] P. Fallavollita and F. Cheriet. Robust coronary artery tracking from fluoroscopic image sequences. In *Proc. of Int. Conf. on Image Analysis and Recognition*, pages 889–898, 2007.

[9] L. M. J. Florack, B. M. ter Haar Romeny, J. J. Koenderink, and M. A. Viergever. Scale and the differential structure of images. *Int. Journal of Image and Vision Computing Special Issue: Information Processing in Medical Imaging*, 10:376–388, 1992.

[10] A. Frangi, W. Niessen, K. Vincken, and M. Viergever. Multiscale vessel enhancement filtering. In *Proc. of Int. Conf. on MICCAI*, pages 130–137, 1998.

[11] M. Garreau, J. L. Coatrieux, R. Collorec, and C. Chardenon. A knowledge-based approach for 3-D reconstruction and labeling of vascular networks from biplane angiographic projections. *IEEE Trans. on Medical Imaging*, 10(2):122–131, 1991.

[12] M. Hart and L. Holley. A method of automated coronary artery tracking in unsubtracted angiograms. In *Proc. of Int. Conf. on Computers in Cardiology*, pages 93–96, 1993.

[13] W. E. Hart, M. Sanjeev Arulampalam, B. Côté, P. Kube, and M. R. Nelson. Automated measurement of retinal vascular tortuosity. In *Proc. of American Symp. on the Medical Informatics Association*, pages 459–463, 1997.

[14] W. E. Hart and M. H. Goldbaum. Registering retinal images using automatically selected control point pairs. In *Proc. of Int. Conf. on Image Processing*, volume 3, pages 576–580, 1994.

[15] A. D. Hoover, V. Kouznetsova, and M. Goldbaum. Locating blood vessels in retinal images by piecewise threshold probing of a matched filter response. *IEEE Trans. on Medical Imaging*, 19(3):203–210, 2000.

[16] C. Kirbas and F. Quek. A review of vessel extraction techniques and algorithms. *Int. Journal of ACM Computing Surveys*, 36:81–121, 2004.

[17] A. Klein, T. K. Egglin, J. S. Pollak, F. Lee, and A. A. Amini. Identifying vascular features with orientation specific filters and b-spline snakes. In *Proc. of Int. Conf. on Computers in Cardiology*, pages 113–116, 1994.

[18] J. J. Koenderink. The structure of images. *Int. Journal of Biological Cybernetics*, 50(5):363–370, 1984.

[19] T. M. Koller, G. Gerig, G. Szekely, and D. Dettwiler. Multiscale detection of curvilinear structures in 2-D and 3-D image data. In *Proc. of Int. Conf. on Computer Vision*, pages 864–869, 1995.

[20] Y. Kong, J. J. Morris Jr, and H. D. McIntosh. Assessment of regional myocardial performance from biplane coronary cineangiograms. *American Journal of Cardiology*, 27(5):529–537, 1971.

[21] S. Kozerke, R. Botnar, S. Oyre, M. B. Scheidegger, E. M. Pedersen, and P. Boesiger. Automatic vessel segmentation using active contours in cine phase contrast flow measurements. *Int. Journal of Magnetic Resonance Imaging*, 10(1):41–51, 1999.

[22] R. Liao, D. Luc, Y. Sun, and K. Kirchberg. 3-D reconstruction of the coronary artery tree from multiple views of a rotational x-ray angiography. *Int. Journal of Cardiovascular Imaging*, 26(7):733–749, 2009.

[23] C. Lorenz, I. C. Carlsen, T. M. Buzug, C. Fassnacht, and J. Weese. Multi-scale line segmentation with automatic estimation of width, contrast and tangential direction in 2D and 3D medical images. In *Proc. of Int. Conf. on Computer Vision, Virtual Reality and Robotics in Medicine and Medial Robotics and Computer-Assisted Surgery*, CVRMed-MRCAS '97, pages 233–242, 1997.

[24] S. Lu and S. Eiho. Automatic detection of the coronary arterial contours with sub-branches from an x-ray angiogram. In *Proc. of Int. Conf. on Computers in Cardiology*, pages 575–578, 1993.

[25] R. Malladi, J. A. Sethian, and B. C. Vemuri. Shape modeling with front propagation: a level set approach. *IEEE Trans. on Pattern Analysis and Machine Intelligence*, 17(2):158–175, 1995.

[26] F. Mao, S. Ruan, A. Bruno, C. Toumoulin, R. Collorec, and P. Haigron. Extraction of structural features in digital subtraction angiography. In *Proc. of Int. Conf. on Biomedical Engineering Days*, pages 166–169, 1992.

[27] B. T. Messmer and H. Bunke. A new algorithm for error-tolerant subgraph isomorphism detection. *IEEE Trans. on Pattern Analysis and Machine Intel.*, 20(5):493–504, 1998.

[28] I. Nwogu and L. Lorigo. Fast temporal tracking and 3D reconstruction of a single coronary vessel. In *Proc. of IEEE Int. Conf. on Image Processing*, pages 537–540, 2007.

[29] M. Orkisz, C. Bresson, I. Magnin, O. Champin, and P. Douek. Improved vessel visualization in MR angiography by nonlinear anisotropic filtering. In *Proc. of Int. Society for Magnetic Resonance in Medicine*, volume 37, pages 914–919, 1997.

[30] R. Poli and G. Valli. An algorithm for real-time vessel enhancement and detection. *Int. Journal of Computer Methods and Programs in Biomedicine*, 52(1):1–22, 1997.

[31] F. K. H. Quek and C. Kirbas. Vessel extraction in medical images by wave-propagation and traceback. *IEEE Trans. on Medical Imaging*, 20:117–131, 2001.

[32] U. Rost, H. Münkel, and C. E. Liedtke. A knowledge based system for the configuration of image processing algorithms. In *Proc. of Int. Conf. on Computational Intelligence and Multimedia Applications*, 1998.

[33] D. Rueckert and P. Burger. Contour fitting using stochastic and probabilistic relaxation for cine MR images. *Int. Journal of Computer Assisted Radiology*, pages 137–142, 1995.

[34] N. Sang, Q. Tang, X. Liu, and W. Weng. Multiscale centerline extraction of angiogram vessels using gabor filters. In *Proc. of Int. Symp. on Computational and Information Science*, volume 3314, pages 570–575, 2004.

[35] J. A. Sethian. A fast marching level set method for monotonically advancing fronts. In *Proc. of American Conf. on National Academy of Sciences*, volume 93, pages 1591–1595, 1995.

[36] G. Shechter, F. Devernay, E. Coste-Maniere, A. Quyyumi, and E. R. McVeigh. Three-dimensional motion tracking of coronary arteries in biplane cineangiograms. *IEEE Trans. on Medical Imaging*, 22(4):493–503, 2003.

[37] C. Smets, G. Verbeeck, P. Suetens, and A. Oosterlinck. A knowledge-based system for the delineation of blood vessels on subtraction angiograms. *Int. Journal of Pattern Recognition Letters*, 8(2):113–121, 1988.

[38] Z. Sun and Weirong Ding. Analysis of coronary arterial dynamics from x-ray angiographic sequences. In *Proc. of Int. Symp. on Computational Intelligence and Design*, pages 201–204, 2009.

[39] B. C. S. Tom, S. N. Efstratiadis, and A. K. Katsaggelos. Motion estimation of skeletonized angiographic images using elastic registration. *IEEE Trans. on Medical Imaging*, 13(3):450–460, 1994.

[40] Y. Tsin, K. Kirchberg, G. Lauritsch, and C. Xu. A deformation tracking approach to 4D coronary artery tree reconstruction. In *Proc. of Int. Conf. on MICCAI*, pages 68–75, 2009.

[41] J. Wang and J. Zhang. An iterative refinement DSA image registration algorithm using structural image quality measure. In *Proc. of Int. Conf. on Intelligent Information Hiding and Multimedia Signal Processing*, pages 973–976, 2009.

[42] Y. Wang, H. Z. Shu, Z. D. Zhou, C. Toumoulin, and J. L. Coatrieux. Vessel extraction in coronary x-ray angiography. In *Proc. of IEEE Conf. on Engineering in Medicine and Biology*, pages 1584–1587, 2005.

[43] C. Xu and J. L. Prince. Generalized gradient vector flow external forces for active contours. *European Journal of Signal Processing*, 71:131–139, 1998.

[44] J. Xu, K. D. Kochanek, S. L. Murphy, B. Tejada-Vera, et al. Deaths: final data for 2007. *National Vital Statistics Reports*, 58(19):1–136, 2010.

[45] J. Yang, Y. Wang, S. Aleksejevs, S. Zhou, Y. Liu, and W. Chen. Multiresolution elastic registration of X-Ray angiography images using Thin-Plate spline. *IEEE Trans. on Nuclear Science*, 54(1):152–166, 2007.

[46] S. Zheng and Y. Daoyin. Tracking vessels in x-ray angiogram sequences based on deformable model. *Iranian Journal of Electrical and Computer Engineering*, 4(2):137–143, 2005.

[47] H. Zhu and M. H. Friedman. Vessel tracking by template string in angiography. In *Proc. of Int. Conf. on Medical Image Acquisition and Processing*, pages 29–33, 2001.

[48] A. Zifan, P. Liatsis, P. Kantartzis, M. Gavaises, N. Karcanias, and D. Katritsis. Automatic 3-D reconstruction of coronary artery centerlines from monoplane x-ray angiogram images. *Int. Journal of Biological Sciences*, 1:44–49, 2008.